International Journal of Extreme Manufacturing

TOPICAL REVIEW • OPEN ACCESS

High-throughput microfluidic production of carbon capture microcapsules: fundamentals, applications, and perspectives

OPEN ACCESS
IOP Publishing | IMMT
International Journal of Extreme Manufacturing
Int. J. Extrem. Manuf. **6** (2024) 032010 (32pp)
https://doi.org/10.1088/2631-7990/ad339c

Topical Review

High-throughput microfluidic production of carbon capture microcapsules: fundamentals, applications, and perspectives

Xiangdong Liu[1], Wei Gao[2], Yue Lu[2], Liangyu Wu[1] and Yongping Chen[1,3,*]

[1] College of Electrical, Energy and Power Engineering, Yangzhou University, Yangzhou, Jiangsu 225127, People's Republic of China
[2] Key Laboratory of Energy Thermal Conversion and Control of Ministry of Education, School of Energy and Environment, Southeast University, Nanjing, Jiangsu 210096, People's Republic of China
[3] Jiangsu Key Laboratory of Micro and Nano Heat Fluid Flow Technology and Energy Application, School of Environmental Science and Engineering, Suzhou University of Science and Technology, Suzhou, Jiangsu 215009, People's Republic of China

E-mail: ypchen@seu.edu.cn

Received 8 August 2023, revised 25 October 2023
Accepted for publication 13 March 2024
Published 4 April 2024

Abstract

In the last three decades, carbon dioxide (CO_2) emissions have shown a significant increase from various sources. To address this pressing issue, the importance of reducing CO_2 emissions has grown, leading to increased attention toward carbon capture, utilization, and storage strategies. Among these strategies, monodisperse microcapsules, produced by using droplet microfluidics, have emerged as promising tools for carbon capture, offering a potential solution to mitigate CO_2 emissions. However, the limited yield of microcapsules due to the inherent low flow rate in droplet microfluidics remains a challenge. In this comprehensive review, the high-throughput production of carbon capture microcapsules using droplet microfluidics is focused on. Specifically, the detailed insights into microfluidic chip fabrication technologies, the microfluidic generation of emulsion droplets, along with the associated hydrodynamic considerations, and the generation of carbon capture microcapsules through droplet microfluidics are provided. This review highlights the substantial potential of droplet microfluidics as a promising technique for large-scale carbon capture microcapsule production, which could play a significant role in achieving carbon neutralization and emission reduction goals.

Keywords: carbon capture, microcapsules, droplet microfluidic, high-throughput production, carbon neutralization

* Author to whom any correspondence should be addressed.

2631-7990/24/032010+32$33.00

1. Introduction

Carbon dioxide (CO_2) is a prominent greenhouse gas contributing significantly to global climate change [1]. CO_2 emissions come from various substantial sources, including fossil fuel combustion [2–4], industrial activities [5] (e.g. steel and mining industries), land-use and agricultural practices [6], transportation [7], and building and construction [8]. Over the past three decades, the mean growth rate of CO_2 has been gradually increasing, underscoring the significance of carbon capture, utilization, and storage (CCUS) as a pivotal approach to mitigate CO_2 emissions [9–11]. Among the CCUS components, carbon capture assumes primary importance as it accounts for over 70% of the overall CCUS cost [12]. Thus, it has become a focal point of extensive research efforts to enhance efficiency and reduce the cost of carbon capture.

Microcapsules have emerged as an important tool for carbon capture. Especially, in recent years, droplet microfluidics method that can precisely generate and manipulate droplets inside microchannels provides a promising approach to create the high-quality carbon capture microcapsules, as shown in figure 1. It can be seen that droplets generated from microfluidic devices are monodispersed, controllable and concentricity, which provide the necessary and versatile templates for the generation of carbon capture microcapsules. These microcapsules can be further fabricated by using interfacial polycondensation on the droplets or directly photocuring the droplets. Subsequently, the microcapsules which have absorbed CO_2 can be heated in the regeneration process to emit high-purity CO_2 that can be compressed for storage or utilization. It is worth noting that the generation performance of droplets, including size, topological structure, throughput and monodispersity, which is affected by the involving microfluidic device configuration and hydrodynamics, directly determines the characteristics of the produced microcapsules. For examples, with the same core diameter, CO_2 capture capacity increases with decreasing shell thickness [13]. Additionally, the mass transfer of CO_2 and solution was also affected by the microcapsule size, and the thermal stability and CO_2 absorption capacity can be adjusted by controlling the core-shell volume ratio of the microcapsules [14, 15]. Over the past two decades, various approaches have been proposed to enhance the production rate of emulsion droplets, primarily focusing on including parallelized microfluidic droplet generators [16–18] and splitting large droplets into smaller batches [19, 20]. However, it is important to note that these methods necessitate precise fabrication of microfluidic devices and delicate wettability modifications of microchannels, which are currently confined to the laboratory development stage [21]. Therefore, it becomes imperative to comprehensively review and summarize the available high-throughput microfluidic approaches, along with the fundamental microfluidic fabrication methods.

This review focuses on the high-throughput production of microcapsules for carbon capture using droplet microfluidics (figure 2). It begins with an overview of different microfluidic chip fabrication technologies, such as wet etching, soft lithography, hot embossing, capillary assembly, and three-dimensional (3D) printing. It then discusses the microfluidic generation of emulsion droplets and the relative hydrodynamic considerations that serve as the basis for achieving microfluidic high-throughput production. Furthermore, a comprehensive assessment of the generation of microcapsules for carbon capture via droplet microfluidics is provided, followed by a forward-looking perspective on the potential for high-throughput. By consolidating and evaluating these key aspects, this review aims to provide an informed and practical guideline for the selection of appropriate high-throughput microfluidic approaches, thereby promoting progress toward the large-scale utilization of microcapsules for carbon capture.

2. Microencapsulated solvents for carbon capture

Microcapsules designed for carbon capture commonly encapsulate a diverse range of solvents, including ionic liquids (ILs), metal-organic frameworks (MOFs), and chemical absorption solvents (figure 3). In the following section, an overview of the distinctive characteristics of these solvents is presented.

2.1. ILs

ILs have garnered significant attention as promising candidates for carbon capture, owing to their remarkable advantages such as negligible vapor pressure, low energy loss, and excellent thermal stability. As ionic compounds that maintain a liquid state at room temperature, ILs offer a unique capture mechanism reliant on weak interactions with CO_2, primarily through physisorption [34, 35]. Notably, the recycling process of ILs entails low energy consumption, as their low thermal absorption requires only 11 $kJ{\cdot}mol^{-1}$ [36]. Initially, ILs are applied in post-combustion capture technology. However, it should be noted that certain ILs can react with CO_2 through chemisorption, affecting CO_2 capture. Additionally, the viscosity of ILs reduces solvent losses but limits mass transfer, resulting in low absorption rates. To address these challenges, researchers have successfully synthesized task-specific ILs by incorporating suitable moieties into conventional ILs, thereby enhancing their absorption capacity. While detailed synthesis methods of ILs have been previously summarized in reviews [37–39], the focus of this review article will lie in exploring the diverse applications of ILs, rather than delving extensively into the synthesis procedures.

In recent studies, the utilization of ionic liquid in carbon capture has been explored with promising results. Liu *et al* [40] investigated the CO_2 conversion efficiency of nanosheet loading with ionic liquid and Co single atom, as shown in figure 4(a-i). It demonstrated that the presence of ionic liquid facilitates electron extraction, offering a feasible strategy for CO_2 conversion. Similarly, Vishwakarma *et al* [41] reported on an interfacial catalytic reaction platform for carbon capture (figure 4(a-ii)), where immobilized ionic liquid catalysts were used in a continuous-flow micro-reactor. This platform

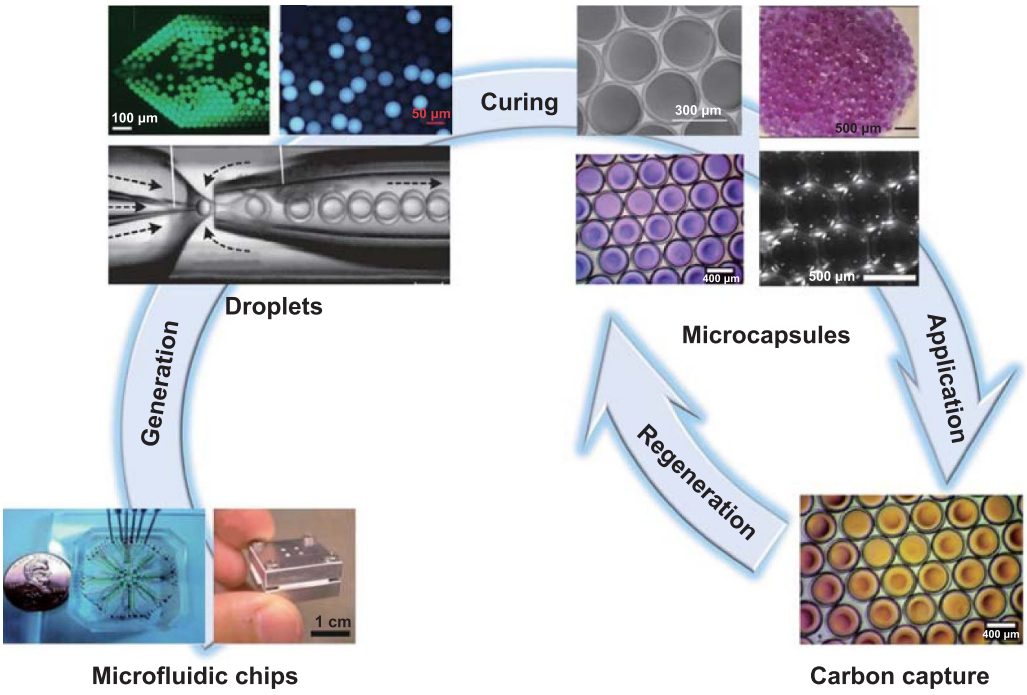

Figure 1. Schematic illustration of the application of carbon capture with microcapsules generated from microfluidic droplets. Reprinted with permission from [22]. Copyright (2011) American Chemical Society. Reproduced from [23] with permission from the Royal Society of Chemistry. Reprinted with permission from [24]. Copyright (2011) American Chemical Society. [13] John Wiley & Sons. © 2022 Wiley Periodicals LLC. Reproduced from [25], with permission from Springer Nature. Reprinted with permission from [26]. Copyright (2011) American Chemical Society.

effectively facilitated CO_2 utilization and enhanced mass transfer. For now, most of the ILs are still studied in the laboratory because of the difficulty in the synthesis of high-throughput of ILs and the high cost [37]. During the industrial process, Chevron Company is a famous institution to use commercial ionic liquid for the capture of CO_2 [42]. The commercial IL used in the industrial process by the Chevron Company is [bmim] [acetate] with 14 wt. % water, which is able to reduce CO_2 greatly in a complex gaseous stream.

2.2. MOFs

MOFs represent a class of crystalline porous materials constructed from multi-metallic units called secondary building units (SBUs) and organic linkers [48]. The final topology structure of the material framework is predominantly determined by the SBUs, making them a critical factor in MOF design. The structure of SBUs depends on several key factors, including the types of metal ions, the structure of organic ligands, the ratio of metal ions to ligands, and the types of solvents [49]. The exceptional porosity and large surface area of MOFs contribute to their high CO_2 adsorption capacity, surpassing that of disordered carbon materials which is less than 2000 $m^2\ g^{-1}$. Some MOFs exhibit surface areas reaching 5000 $m^2\ g^{-1}$ or even higher [50]. Moreover, the unsaturated metal ligands of MOFs usually have a pH above 7, further enhancing their CO_2 adsorption capacity. For example, MOF-74 demonstrates a remarkable CO_2 adsorption capacity of up to 6.25 $mmol{\cdot}g^{-1}$ at 25 °C and 1 bar [51]. To improve their surface area, porosity, and thermal stability, the regulation of orifice shape, orifice size, and the choice of materials can be effectively employed [52]. Despite these advantageous properties, the practical industrial application of MOFs is impeded by their poor stability and tendency to form powders. Therefore, a viable strategy to overcome these challenges involves combining MOFs with other materials such as metallic nanoparticles, graphene, and metal oxides, which can enhance their stability and facilitate industrial application.

Nandi *et al* [43] reported an ultra-microporous MOF, with a structure shown in figure 4(b-i). This MOF exhibited remarkable CO_2/H_2 selectivity and demonstrated CO_2 is self-diffusivity. The unique ultra-microporous architecture ensured exceptional stability, even in the presence of humid gas streams. In another study, Kumar *et al* [44] investigated the CO_2 adsorption capabilities of five different materials (figure 4(b-ii)). The evaluation involved various techniques, such as temperature-programmed desorption, thermogravimetric analysis and mass spectrometry (MS). Among the tested materials, MOFs, HKUST-1 and Mg-MOF-74, exhibited relatively high adsorption capacities. However, these MOFs showed sensitivity to humidity, presenting a challenge for their future application in carbon capture. Furthermore, Liang *et al* [45] presented a Cu (II) MOF characterized by a high density of active sites (figure 4(b-iii)), which demonstrated impressive CO_2 adsorption performance, with a high volumetric uptake of 171 $cm^3{\cdot}cm^{-3}$ under ambient conditions.

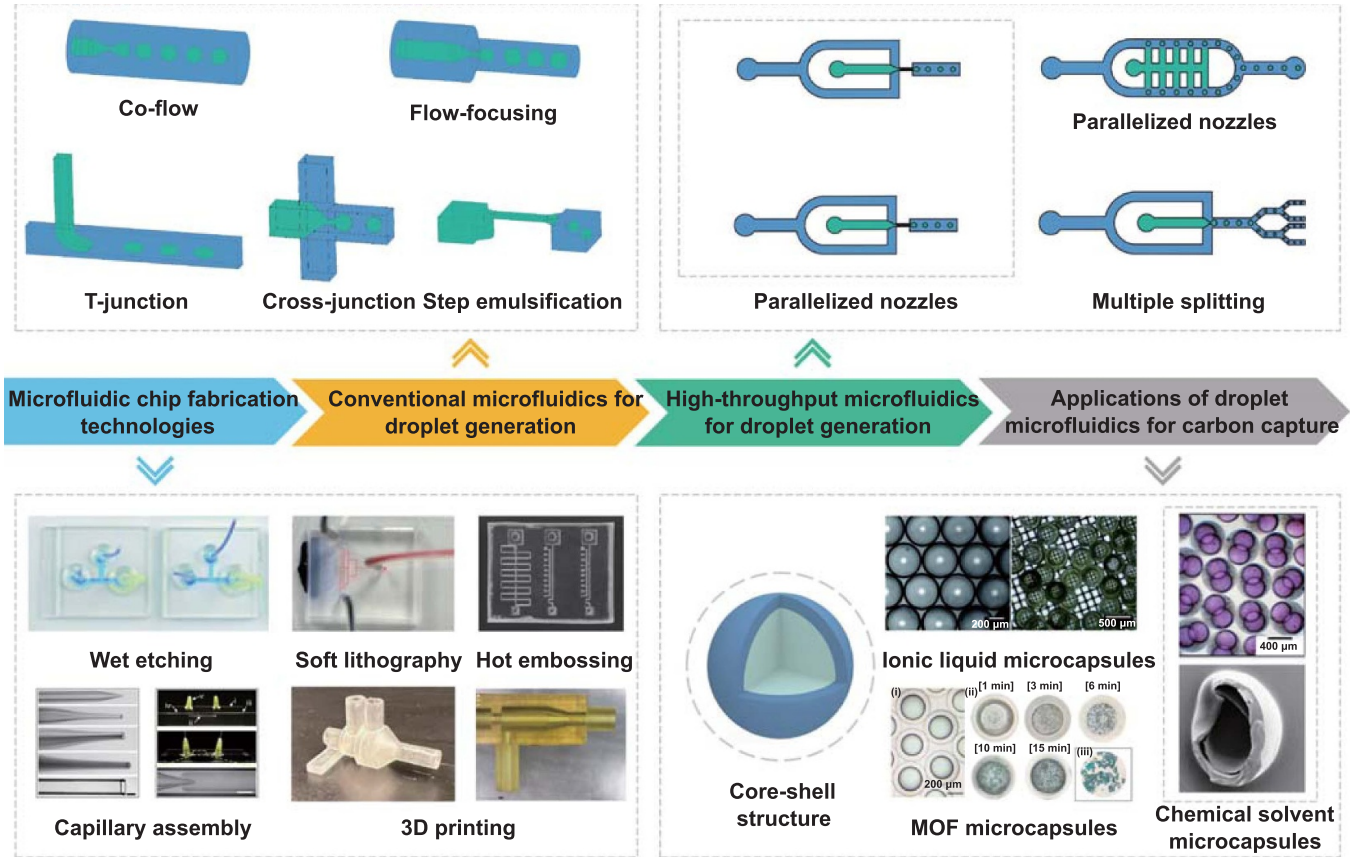

Figure 2. An overview of the themes discussed in this review, from microfluidic chip fabrication technologies to applications of droplet microfluidics for carbon capture. Reproduced from [27] with permission from the Royal Society of Chemistry. Reproduced from [28], with permission from Springer Nature. Reproduced from [29] with permission from the Royal Society of Chemistry. Reproduced from [30], with permission from Springer Nature. Reprinted from [31], © 2020 Elsevier Ltd All rights reserved. Reproduced from [32] CC BY 4.0. Reproduced from [33] with permission from the Royal Society of Chemistry. Reprinted from [14], © 2021 Institute of Process Engineering, Chinese Academy of Sciences. Publishing services by Elsevier B.V. on behalf of KeAi Communications Co., Ltd. [13] John Wiley & Sons.© 2022 Wiley Periodicals LLC.

Zeolite 13X is one of the most common commercial MOFs in the industrial carbon capture application. Especially, the isostatic heat of adsorption for CO_2 by the Zeolite 13X is 37.2 kJ mol^{-1}, which is much higher than that of nitrogen and methane [53].

2.3. Chemical absorption solvents

The chemical reaction with an alkaline solution has proven to be an effective method for CO_2 absorption, owing to the acidic nature of CO_2. This reaction leads to the formation of a weakly bonded intermediate compound, which can subsequently be regenerated [54]. The ideal chemical solvent for CO_2 absorption exhibits several key characteristics, such as high reactivity with CO_2, a large absorption capacity, high thermal stability, low regeneration cost, minimal environmental impact, and cost-effectiveness. Currently, commercial chemical absorption solvents used for the carbon capture are applied into the post-combustion and pre-combustion capture technologies [55]. These solvents are most used in industry for carbon capture. Monoethanolamine (MEA), one most used commercial chemical absorption solvent, has a fast reaction rate with CO_2 and its removal ratio of CO_2 is able to keep high even at the low CO_2 concentration. However, the corrosivity and regeneration energy requirement of MEA are high, which is unfavorable for the industrial application [56]. Another chemical solvent, Selexol, is able to capture CO_2 in a combined cycle power plant [57]. In addition, piperazine (PZ)-promoted potassium carbonate (K_2CO_3), and concentrated aqueous PZ are also belonged to the commercial solvents for the industrial carbon capture applications [58].

Amine-based solvents are classified into primary, secondary, or tertiary, depending on the degree of nitrogen atom substitution [59]. For example, MEA represents a typical primary amine, characterized by one alkanol chain and two hydrogen atoms bonded to a nitrogen atom. Primary and secondary alkanol amines exhibit rapid reactivity with CO_2, forming carbamates, while tertiary alkanol amines require the facilitation of the CO_2 hydrolysis reaction to yield bicarbonates [59]. The heat of the reaction involved with bicarbonate formation is lower than that of carbamate formation, making tertiary amines often blended with primary or secondary amines

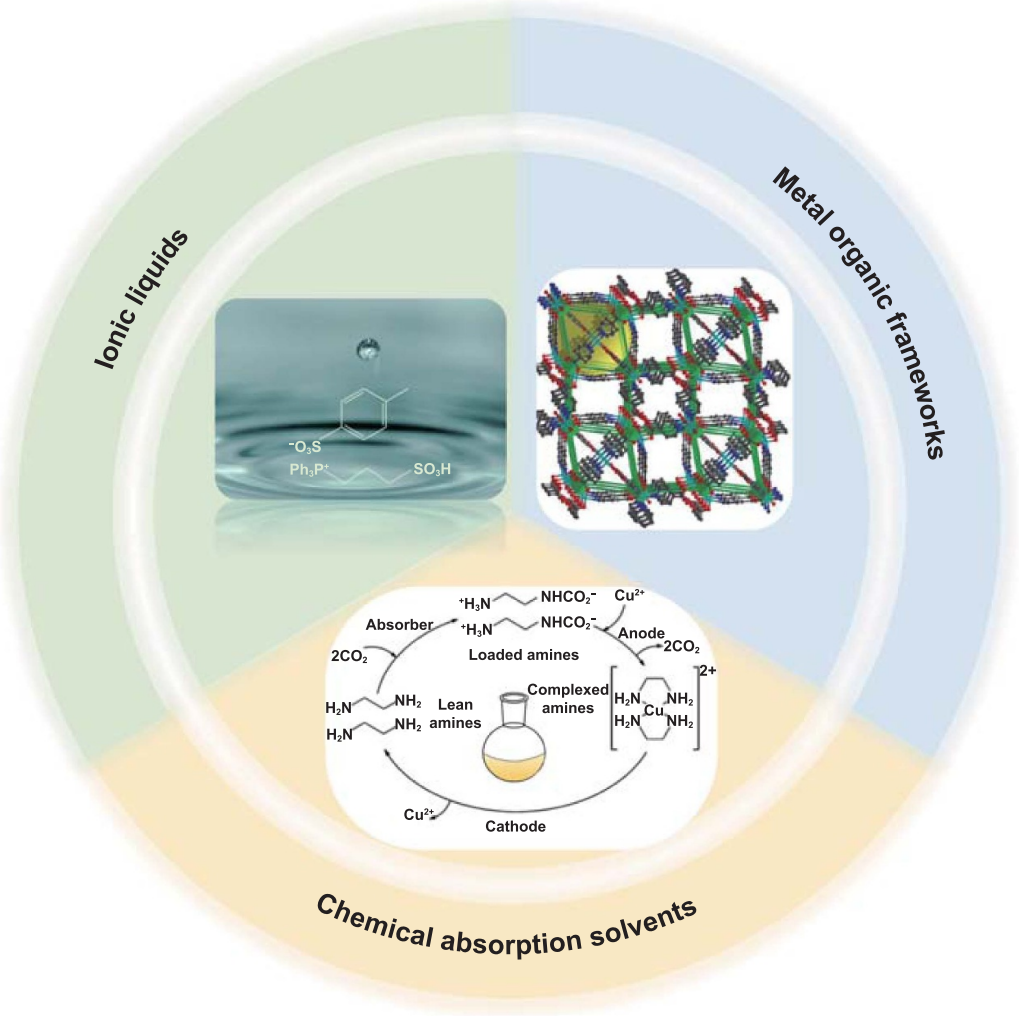

Figure 3. Microencapsulated solvents for carbon capture.

to reduce solvent regeneration costs. Despite MEA being a relatively economical and well-established industrial technology, it faces certain challenges, including solvent degradation, high energy consumption during regeneration, and equipment corrosion [60]. Therefore, exploring alternative solvents with higher CO_2 capacity and lower energy consumption is of paramount importance.

Three classes of amine-modified sorbents based on their respective preparation methods are summarized (figure 4(c-i)) [61]. Class 1 sorbents are prepared through physical impregnation, while Class 2 sorbents are produced via covalent tethering using silane linkage. Generally, Class 1 sorbents exhibit higher CO_2 capacity compared to Class 2 sorbents, owing to their higher amine content. Class 3 sorbents, on the other hand, are prepared through direct covalent tethering via in-situ polymerization. In an insightful study, Gebald *et al* [62] introduced a novel amine-based nano-fibrillated cellulose and investigated its CO_2 absorption/desorption process. The material demonstrated exceptional stability over 100 cycles, with a reduction in CO_2 absorption capacity of less than 5%. Sculley and Zhou [46] added zirconium content to the complex amine-supported porous silica systems for carbon capture (figure 4(c-ii)), which improved desorption kinetics effectively. Furthermore, as shown in figure 4(c-iii), amine solvents were combined with MOFs to realize the chemisorption of CO_2 [47].

In summary, the unique combination of low vapor pressure and high thermal stability makes ILs highly advantageous for applications in carbon capture. MOFs exhibit high surface area and CO_2 adsorption capacities, rendering them favorable candidates for carbon capture. Chemical absorption solvents, on the other hand, are widely used in the industry due to their cost-effectiveness. As a result, these three types of solvents are commonly utilized in carbon capture processes. However, besides the advantages, these solvents also have some certain limitations, including restricted mass transfer and absorption rates, which are summarized in table 1. It is benefit to enhance mass transfer and improve absorption rates with the encapsulation of these solvents, so that droplet microfluidics is an effective tool for carbon capture.

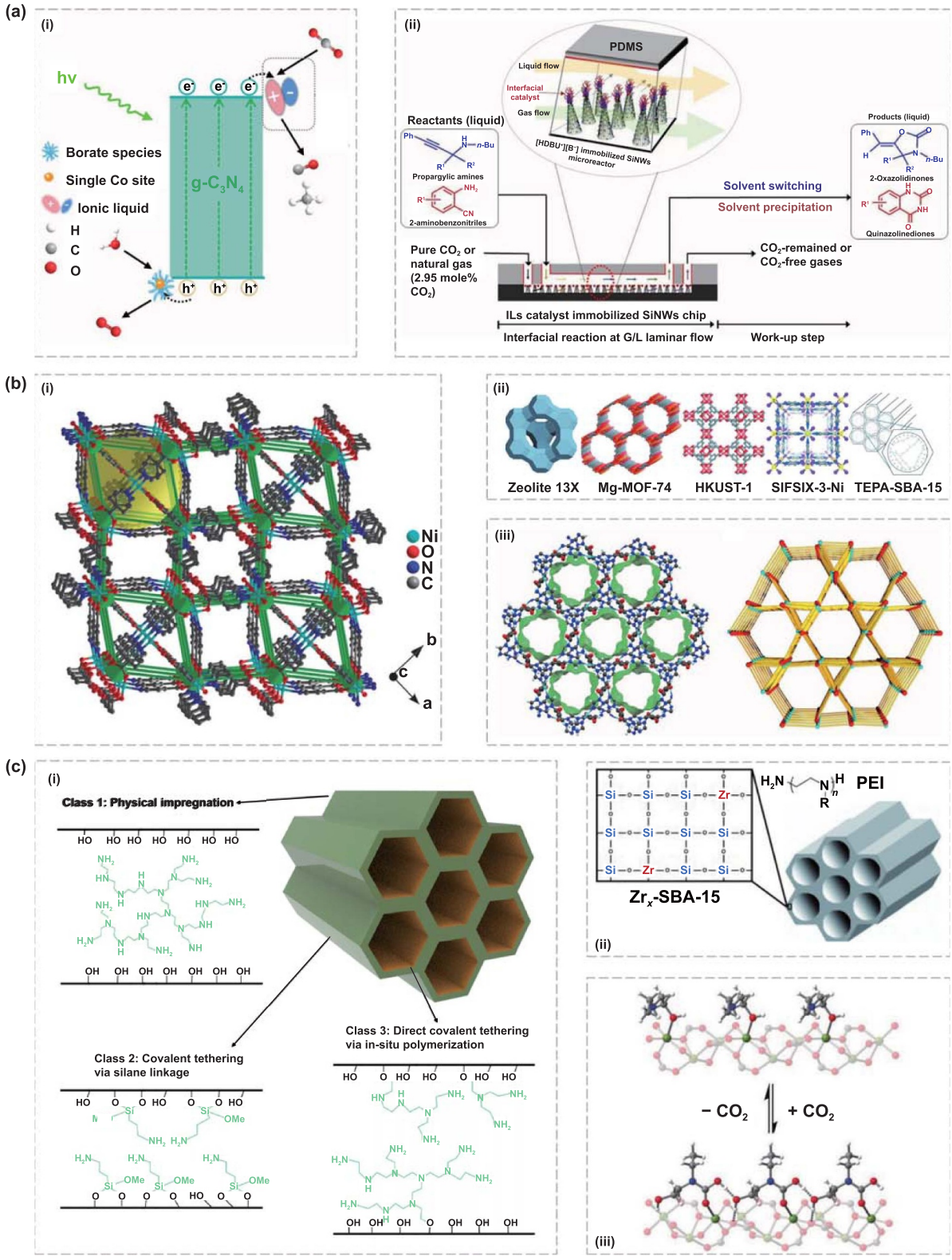

Figure 4. Schematic illustration of the microencapsulated solvents: (a) ILs applied for carbon capture. (i) Illustration of the proposed photo catalytic mechanism of CO_2 photo conversion over IL/Co bCN. Reproduced from [40]. CC BY 4.0; (ii) an integrated gas-liquid microfluidic system and overall process for carbon capture. Reproduced from [41]. CC BY 4.0. (b) MOFs applied for carbon capture. (i) A single-crystal structure of MOFs generated using OLEX. From [43]. Reprinted with permission from AAAS; (ii) five materials investigated for their ability to adsorb CO_2. [44] John Wiley & Sons.© 2015 WILEY-VCH Verlag GmbH & Co. KGaA, Weinheim; (iii) the structure of acid-base resistant MOFs for carbon capture. Reproduced from [45]. CC BY 4.0. (c) Chemical absorption solvents for carbon capture. (i) Three classes of amine-modified sorbents; (ii) representation of an SBA-15 support with incorporated zirconium ions. [46] John Wiley & Sons.Copyright © 2012 WILEY-VCH Verlag GmbH & Co. KGaA, Weinheim; (iii) a metal–organic framework functionalized with structurally diverse alcoholamines and alkoxyalkylamines. [47] John Wiley & Sons.© 2019 Wiley-VCH Verlag GmbH & Co. KGaA, Weinheim.

Table 1. The summary and comparison of microencapsulated solvents for carbon capture.

Solvents	ILs	MOFs	Chemical absorption
Absorption mechanism	Physisorption (mainly)	Physisorption	Chemisorption
Stability	Good thermal stability	Poor stability	Good stability
CO_2 capacity	Low	High	High
Cost	Low energy consumption	High	Low
Advantages	Solvents loss reduction; Negligible vapor pressure	High surface area; Porosity	Widely used into industry
Disadvantages	Limited mass transfer;	Powder statement; Hard to be applied into industry	Solvents degradation; High energy consumption; Equipment corrosion
References	[34–36]	[49, 50]	[59, 60]

3. Microfluidic chip fabrication technologies

The fabrication of microfluidic devices plays a fundamental role in droplet microfluidics. A high degree of integration, specific geometric structures, and physicochemical features, such as surface properties and basic materials, are all critical considerations in the design of microfluidic devices. When designing microfluidic devices for droplet formation, it is important to take into account the various characteristics of available fabrication methods, such as transparency, channel wettability, pressure resistance, cost, temperature resistance, and more. The important fabrication methods, including wet etching, soft lithography, hot embossing, capillary assembly and 3D printing are introduced briefly.

In wet etching method, micromachined microfluidic devices based on glass/silicon substrates are extensively utilized. These substrates possess several advantages, including high thermal stability and effective solvent resistance, making them suitable for use in high-temperature and organic environments [63–65]. Additionally, the transparency of glass facilitates the observation of droplet formation in the microfluidic devices. However, the properties of glass and silicon also present challenges during the preparation and application process, such as brittleness and gas impermeability. The typical procedure of micromachining of glass/silicon is illustrated in figure 5(a). The resulting microchannels are quasi-two-dimensional, making them easy to fabricate in parallelized microfluidic droplet generators. However, large-scale production of glass and silicon microfluidic devices also requires overcoming several impediments such as high costs and the need for clean-room equipment.

Rapid prototyping is another widely used fabrication method for the microfluidic device, with PDMS-based soft lithography being the most commonly used approach. PDMS-based soft lithography is notable for its speed and cost-effectiveness, and the substrate can be reusable for mass production and industrial applications [71]. The typical procedure of PDMS-based soft lithography involves several steps as shown in figure 5(b). The transparency of PDMS microfluidic devices makes them favorable for experimental visual observation as well. The entire fabrication process is carried out under mild conditions because PDMS can be cured at low temperatures and does not release hazardous substances, making it a convenient and eco-friendly option. Nevertheless, PDMS-based soft lithography also has its limitations. For examples, the wettability of PDMS needs to be modified for successful droplet formation, and the modified wettability is not always long-lasting. Additionally, the bonding part cannot withstand the high pressure in the microchannel of the device, so there is a risk of fluid leakage when using a working fluid with high viscosity. Moreover, there are limitations in the applications of the PDMS microfluidic devices for organic materials owing to the swelling of PDMS and the deformation of the microchannels [72–76]. Compared to the micromachining of glass/silicon, PDMS soft lithography is more widely used for water-in-oil (W/O) droplet formation because of its inherent hydrophobicity [77]. It is worth noting that PDMS-based soft lithography is convenient for the mass production of droplet generation since microfluidic devices are highly replicable.

The hot embossing technology is often used to fabricate microfluidic devices based on polymethyl methacrylate (PMMA) for visualized droplet generation. PMMA is a widely used amorphous thermoplastic [78]. The hot embossing process involves heating the silicon mold and PMMA sheet, pressing the mold into the PMMA sheet to transfer the patterns, cooling the pattern-carrying PMMA, and finally bonding a transparent cover onto the PMMA substrate for visualization (figure 5(c)) [79, 80]. Similar to PDMS, PMMA is naturally hydrophobic, making it suitable for producing W/O emulsions without the need for surface modification. There is a risk that PMMA can collapse during hot embossing, which can affect the reliability of droplet generation. In particular, if the reservoir in a step emulsification device collapses, the confinement gradient during droplet generation will be destroyed, leading to emulsification failure. Therefore, although PMMA-based hot embossing lithography is an available alternative to PDMS-based soft lithography, it is currently less popular in the laboratory.

Microfluidic devices fabricated by above methods are typically quasi-two-dimensional planar structures. Consequently, the droplets generated in these microchannels can easily contact with the channel walls, and in the worst case, collapse and stagnate due to their better wettability than the continuous

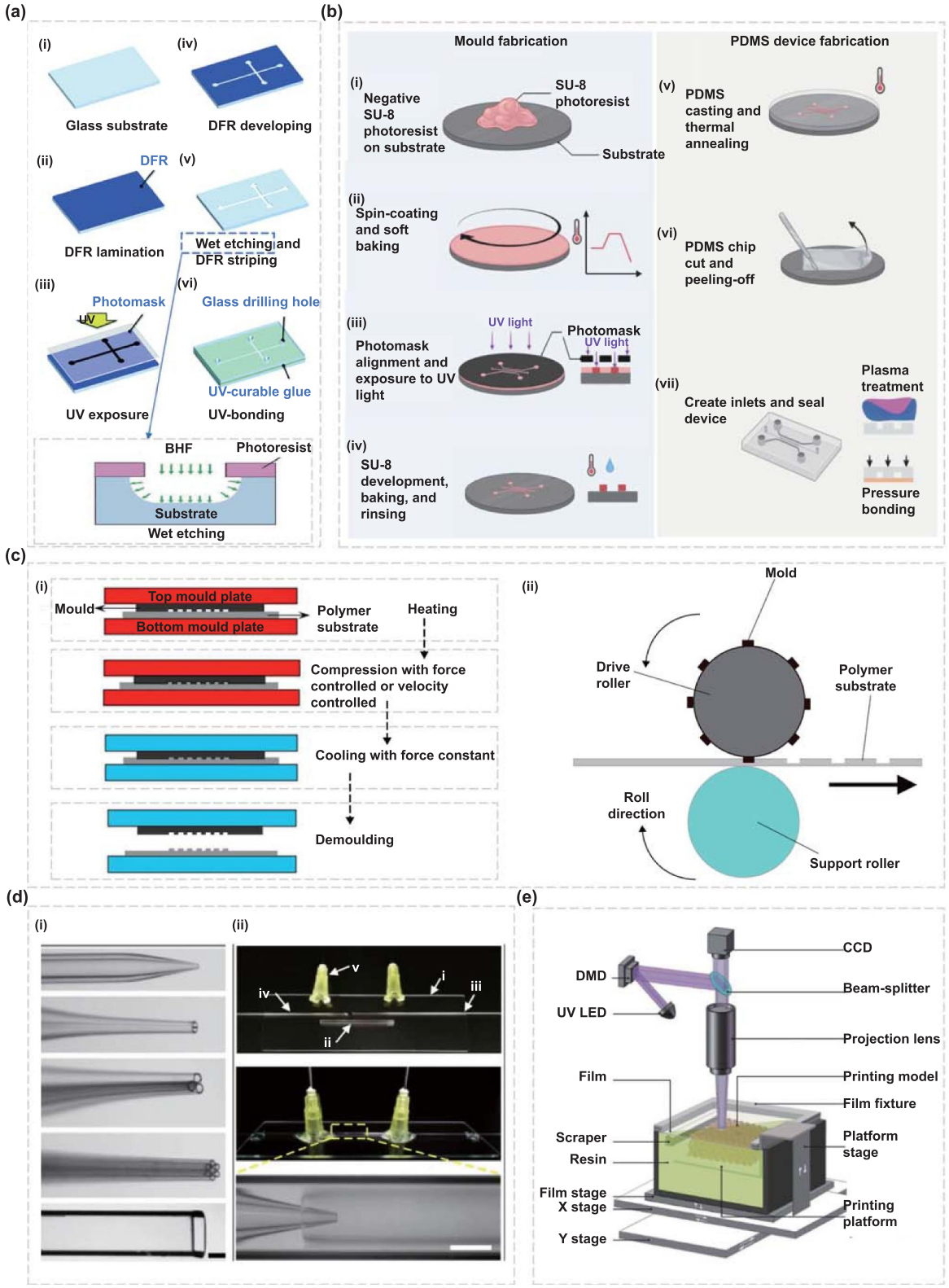

Figure 5. Schematic illustration of the process for fabricating glass microfluidic devices by (a) wet etching. Reproduced from [27] with permission from the Royal Society of Chemistry. [66] John Wiley & Sons.© 2018 WILEY-VCH Verlag GmbH & Co. KGaA, Weinheim; (b) soft lithography. Reproduced from [67]. CC BY 4.0; (c) hot embossing process: (i) conventional and (ii) roller to roller. Reprinted from [68], © 2019 Elsevier Ltd All rights reserved. Selection and peer-review under responsibility of the scientific committee of the 10th International Conference of Materials Processing and Characterization, Reproduced from [69]. © IOP Publishing Ltd All rights reserved; (d) capillary assembly: (i) capillaries with different structures; (ii) photo of capillary microfluidics assembly. Reproduced from [30], with permission from Springer Nature. (e) 3D printing. Reproduced from [70]. © The Author(s). Published by IOP Publishing Ltd CC BY 4.0.

phase. To avoid such problems, wettability modification of the microchannel is necessary, particularly during microfluidic droplet generation. However, selectively modifying specific parts of microchannels in these microfluidic devices remains a challenge. The 3D microchannels fabricated through the modular assembly method allow for the localized wettability treatments to be performed separately on different modules, making it easier to fabricate devices with multiple levels of droplet generators. Currently, the most widely used modular assembly method for manufacturing microfluidic devices is the glass capillary-based method, owing to its low cost, easy fabrication, and simple operation. A typical counter-flow flow-focusing microfluidic device is fabricated by nesting cylindrical glass capillary tubes within a square glass tube with matched size, which achieves good coaxial alignment for the preparation of microscale emulsion droplets and other derived functional materials (figure 5(d)) [81–83]. These devices can typically withstand higher pressure. However, it is worth noting that the structure of the capillary tip is still usually handmade via hot drawing, which limits the reproducibility and scalability of the microfluidic devices.

The use of 3D printing has gained popularity in recent years as a technique for directly fabricating 3D structures in a single step [84–86]. The 3D geometric information is stored in a graphic program file and automatically processed by a computer-controlled printer system, enabling accurate and high-resolution fabrication with low time consumption and cost. This technique is also environmentally friendly due to the minimal production of redundant parts during the fabrication process. Additionally, with the integration of industrial-grade user interfaces and embedded control systems, the commercialization of 3D printing technology has promising development prospects. Among various available types of 3D printing techniques, stereolithography (STL) is particularly favorable for microfluidic device fabrication due to its ability to generate small and complex channel structures that are difficult to realize using other methods [87, 88]. STL, an additive manufacturing process, involves slicing the 3D model of STL format and printing the photosensitive resin layer by layer using a laser beam [89–91]. As shown in figure 5(e), a lifter moves the printing platform up and down, ensuring sufficient curing time for the photosensitive resin. It is worth noting that the cost of 3D printing increases significantly with the miniaturization and complexity of microchannels structures. Additionally, the availability of suitable photosensitive resin for 3D printing is still limited, indicating that 3D printing technology is in its infancy yet [70, 92].

Herein, table 2 lists the summary and comparison of various fabrication methods for the microfluidic devices used in droplet generation, aiming to provide suggestions for appropriately performing the microfluidic device fabrication under different conditions. In general, wet etching and soft lithography have proven to be suitable for manufacturing the microfluidic devices for high-throughput droplet generation. Thus, the following sections are mainly focused on these two methods. Ultimately, the selection of a suitable fabrication method for microfluidic droplets generation should consider various factors according to the specific experimental requirements and application needs, such as cost, manufacturing difficulty, reliability, applicability, and droplet formation performance.

4. Microfluidics for droplet generation

4.1. Single-phase droplets

Microfluidic droplet generation is a process that depends on precise flow control of the different phases, which is closely related to the microfluidic geometries used. Based on the flow characteristics of different phases, microfluidic geometries are typically classified into five geometries: co-flow, flow-focusing, T-junction, cross-flow, and step emulsification (figure 6(a)). The first four geometries rely on the viscous shear force to generate droplets, and are thus known as shear-based geometries. In contrast, step emulsification achieves droplet generation through a confinement change in the channel structure, offering a low-energy consumption approach for droplet formation. Droplets with characteristics of monodisperse, controllable and concentricity are necessary versatile templates for production of microcapsules. In order to generate the droplet templates with these characteristics, droplet microfluidics is an effective technology. Hence, it is necessary to investigate and understand the hydrodynamics of the microfluidic droplet generation process, so as to manipulate the generation of droplets. Note that, as for the understanding of the hydrodynamics underlying the microfluidic droplet generation, the hydrodynamics of single-phase droplet formation process is the base for comprehension of the double emulsion droplet formation process. Therefore, even though the majority of the microcapsules are generated from the curing of double emulsion droplets, it is meaningful to introduce the hydrodynamics of single-phase droplet formation as follows.

4.1.1. Conventional microfluidic generation of single-phase droplets. In co-flow streams, the dispersed phase and continuous phase flow in the same direction through the inner and outer channels, respectively. The dispersed phase is pinched off by the continuous phase due to the viscous forces, resulting in droplet formation. The minimum droplet size formed in the co-flow stream can reach several hundred nanometers, while the most common size of droplets in references is between 200 μm–1000 μm [93–96]. The generation frequency of droplets in co-flow configurations typically spans from several hundred Hz to tens of kHz. In the dripping regime, the coefficient of variation (C.V.) of droplets is typically below 3%, indicating a state of monodispersity. During the dripping regime, the viscous force imposed by the continuous flow exceeds the interfacial tension, leading to the detachment of the dispersed phase from the tip and the formation of droplets. As the flow rate of the continuous phase increases, the Capillary number of continuous phase (Ca_o) increases, resulting in a reduction in droplet size. When $Ca + We \approx 1$, a transition from dripping to jetting occurs, revealing different

Table 2. The summary and comparison of various fabrication methods.

Fabrication methods	Wet etching	Soft lithography	Hot embossing	Capillary assembly	3D printing
Materials	Glass/Silicon	PDMS	PMMA	Glass capillary	Photosensitive resin
Wettability	Hydrophilic	Hydrophobic	Hydrophobic	Hydrophilic	Depending on the resin materials
Surface modification	Coated with a hydrophobic agent	Immersed in deionized water	Immersed in deionized water	Coated with a hydrophobic agent	No extra modification with appropriate materials
Manufacturability	1. Need clean-room equipment to manufacture; 2. Easy to manufacture	1. Fast to fabricate; 2. Reusable for mass production;	Fast to fabricate	Ease of fabrication	Easy to fabricate the small and complex structure
Cost	High costs	Cost-effective	Cost-effective	Low costs	High costs with the miniaturization and complexity of microchannels
Advantages	1. Transparent for observation; 2. High thermal stability; 3. Effective solvent resistance; 4. Good thermal conductivity; 5. Electroosmotic flow stability	1. Transparent for observation; 2. Convenient and environmental	1. Transparent for observation;	1. 3D axisymmetric structure; 2. Allow for localized wettability; 3. Simplicity of operation; 4. Withstand high pressure	1. Low time consumption; 2. Environmental-friendly
Disadvantages	1. Brittleness; 2. Gas impermeability;	1. Limitation in withstanding high pressure; 2. Fluid leakage risk using a fluid with high viscosity; 3. Swelling of PDMS and deformation with organic materials	1. Risk of PMMA collapse during hot embossing	1. Manufactured by hand; 2. Limit the reproducibility and scalability	1. Limited suitable photosensitive resin considering pressure or temperature
References	[63–65]	[73, 74, 76]	[78]	[81, 83]	[87, 88]

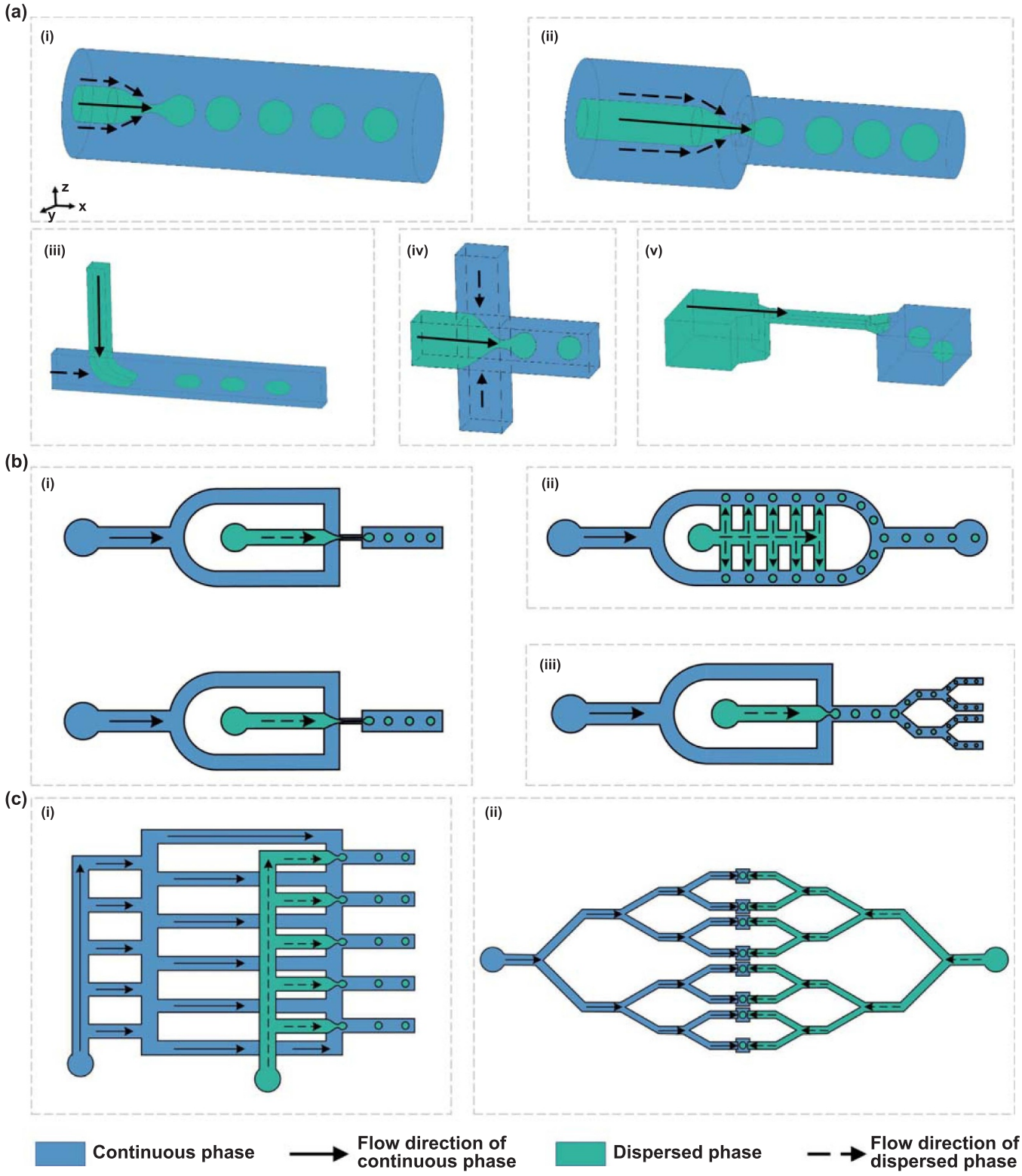

Figure 6. Schematic illustration of microfluidic characteristics: (a) flow behaviors in different droplet generators: (i) co-flow, (ii) flow-focusing, (iii) T-junction, (iv) cross-junction, (v) step emulsification. (b) The scale-up strategies for microfluidic process: (i) parallel numbering-up the nozzles for dispersed phase and continuous phase; (ii) parallel numbering-up the nozzles for dispersed phase; (iii) splitting the emulsion droplets. (c) The fluids distribution network in two common layouts: (i) ladder network and (ii) tree network.

jetting regimes determined by the distinct dominant forces [97]. At high flow rates of the continuous phase, the dominant force is the viscous force from the continuous phase, leading to the formation of a narrow jetting regime. Conversely, at high flow rates of the dispersed phase, dispersed phase inertia becomes the dominant force, resulting in a wide jetting regime.

Further research indicates that jetting occurs when $We_i > 1$ and $Re_i > 1$, or when the $Ca_i > 1$ in the opposite case [98].

Similarly, in flow-focusing geometry, two immiscible fluids flow coaxially with a small orifice configured. Under the effect of hydrodynamic focusing, the dispersed phase is forced through the orifice to facilitate droplet formation. The formation of droplets is influenced by various factors, including fluid flow rates, geometrical parameters, and the fluids' interaction [99–101]. In most 3D flow-focusing devices fabricated by the capillary assembly method, the fluids are induced in a counter-flow condition [24, 102–104]. The fluids can also be induced concurrently, for example, Takeuchi *et al* [105] fabricated the symmetric flow-focusing device by the cast molding method. In quasi-2D flow-focusing devices, the fluids flow in the same direction [106–109]. The minimum droplet size in a flow-focusing device can reach hundreds of nanometers, similar to those in co-flow devices [106, 110]. However, the common size of droplets formed in references is below 100 μm, which is smaller than that in co-flow devices with similar geometric characteristics. This is due to the strong confinement of the flow-focusing orifice, which results in most droplets being of the same magnitude as the orifice radius or smaller [106]. The frequency of droplets generated in flow-focusing devices is similar to that in co-flow devices. However, the interface is unstable due to the continuous phase flowing through the focusing orifice, resulting in abrupt velocity variations. Consequently, the C.V. of droplets produced by flow-focusing devices is slightly higher than that produced by co-flowing devices under the same flow conditions. The typical C.V. of droplets produced by flow-focusing is still below 5% satisfying the monodispersity requirement of most applications. In a 2D microfluidic flow-focusing device, the dispersed phase forms a spherical head due to the influence of interfacial tension. However, when the droplet size exceeds the channel depth, the spherical droplet becomes confined and takes on a disc-shaped form. As the droplet continues growing, a balance is reached between the detaching forces and the holding force acting on the droplet. Under the circumstance that detaching force surpasses the holding force, the interface of droplet collapses to form a droplet.

In the T-junction flow category, two fluids meet at a junction with a vertical angle. The buildup of pressure upstream leads to a breakup once the dispersed phase obstructs the main channel through which the continuous phase flows [111]. If the stream of the continuous phase bypasses the dispersed phase, the system is shear-dominated, where the dispersed phase is sheared by the continuous phase [112]. The neck then breaks into droplets, and the fluid tip retracts to the inlet due to the interfacial tension force [111]. K-junction flow [113] or V-junction flow [114] are variants of the T-junction device that offer flexible flow arrangement. The common droplet size in T-junction devices ranges from 40 μm and 500 μm. In the dripping regime of T-junction cross-flow, droplet size is mainly determined by the viscous shear force, which is proportional to Ca_o.

In the cross-junction flow, the dispersed phase is flanked by the continuous phase from two directions to form droplets. The cross-junction flow is regarded as the flow-focusing flow in some research, while the cross-section decreases in flow-focusing flow, which is unchangeable in the cross-junction flow [115–117]. In cross-junction flow, the fluid tip partially plugs the exit due to the existence of a thin film of the continuous phase [118, 119]. The process of droplet formation is affected by a mechanism in which the competition between the shear stress and interfacial tension forces plays a dominant role. This mechanism is similar to that in the T-junction device, so this structure is difficult to classify as a flow-focusing device. The droplet size is typically over 10 μm and is mainly influenced by the channel structure, while the C.V. is below 2%. The angle between the continuous phase and the dispersed phase is variable in cross-junction flow [120–122].

Monodispersity is generally guaranteed by adjusting flow rates in these shear-based geometries in the dripping regime. Compared with shear-based geometries, the step emulsification device with optimized nozzles weakens the effect of fluid flow rates. As mentioned above, the formation of droplets in step emulsification is a low-energy input way, and the droplet size is insensitive to flow rates [123, 124]. Hence, the step emulsification device is widely used in the high-throughput production of droplets [125].

In a step emulsification process employing a wedge-shaped channel to connect a reservoir, the dispersed phase forms a tongue-shaped interface within the wedge-shaped channel [126]. As the interface enters the reservoir, the tip of the bulb expands and connects with the neck through the liquid thread in the nozzle. With the continuous phase flowing back to the nozzle, the width of the neck gradually decreases until the dispersed phase breaks into droplets. The bulb's expansion is driven by the Laplace pressure difference between the high-curvature interface in the narrow channel and the low-curvature interface in the reservoir, and the filling process is controlled by the balance between viscous forces and surface tension. The pressure difference is related to the curvature difference of the liquid-liquid interface. As the bulb fills, its curvature decreases, leading to a reduction in the internal pressure. Consequently, the pressure drop increases, resulting in an increasing flow from the neck into the bulb. When Q_o exceeds the flow flowing into the nozzle Q_i, the neck width shrinks to the critical value. The neck becomes unstable and collapses quickly as soon as it detaches from the walls of the nozzle. The size of the droplet is determined by the initial wetting regime, and the contact angle of the fluid plays a crucial role.

4.1.2. High-throughput microfluidic generation of single-phase droplets. The production rate for a single droplet maker typically ranges from tens to hundreds of microliters per minute, rendering it unsuitable for industrial applications [127]. To address this limitation, the scale-up strategies for microfluidic process, including the parallelization of microfluidic droplet generation units [128] and multiple splitting of emulsion droplets [129], have been proposed to enhance productivity.

Individual and connected microfluidic droplet generation units have been integrated into one device (figure 6(b-i)).

This allows for independent regulation and minor disturbance between units, resulting in products with different compositions [130]. However, the cost and complexity of this approach of integrating numerous stand-alone pumps limit the practicality of this approach. An alternative strategy involves distributing the dispersed phase in a multi-channel structure (figure 6(b-ii)). This structure is more compact and beneficial for minimizing the device. Due to the interconnection between channels, the even distribution of dispersed phases is vital in this configuration. One blocked channel will result in inhomogeneous fluid distribution, which may lead to polydisperse droplets and is unfavorable for the reliability of high-throughput droplet generation. In contrast to the parallelization strategy, multiple splitting of droplets involves generating emulsion upstream, and then stepwise splitting them through hierarchical junctions (figure 6(b-iii)) [131]. This passive breakup can be repeated without a significant increase in C.V. until droplet radii decrease to approximately the same order as the channel width, resulting in higher yield and reliability [129].

Fluid distribution is critical for realizing mass production at an industrial scale, as uneven flow rates can lead to variations in residence time, mass, and heat transfer [132]. The multi-channel network is specifically designed to ensure even flow rates in each unit, which is particularly important for maintaining droplet monodispersity in shear-based geometries (figure 6(b)). Two common microfluidic channel layouts are the tree-type and ladder-type networks (figure 6(c)). In the tree-type network, the number of branch channels increases by a factor of two between consecutive levels, resulting in a total number of branches equal to 2^n, where n is the level of the tree [133]. Conversely, the ladder-type network consists of several parallel branches connected to a main channel, and the number of branches is arbitrary. While the design of the ladder-type network is more compact and less affected by manufacturing deviations, the tree-type network is more energy efficient. Therefore, it is important to carefully consider the choice of the network when designing microfluidic channels.

Flow-focusing generators and step-emulsification units are suitable parallelization units for droplet generation at an industrial scale. To minimize the C.V. of droplet size in parallelized flow-focusing devices, Hashimoto *et al* [134] investigated the intersection mechanism among four coupled flow-focusing generators, uncovering the compressibility of the dispersed phase and variations at the flow-focusing orifices under pressure. In a similar study, Li *et al* [135] explored the geometric coupling between integrated four parallel generators and the influence of variations in the dimensions of microchannels (figure 7(a)). Meanwhile, Kang *et al* [28] utilized a tree-type network with three layers of fluid distributors in the preparation of nanoparticles to prevent aggregation and clogging, which could lead to the failure of the device. Nisisako and Torii [18] presented a circular arrangement module consisting of 128 junctions, which integrated more droplet generator units on one chip, resulting in reduced consumption of the continuous phase (figure 7(b)). The devices successfully produced monodisperse droplets (C.V. $< 4\%$) and were also applied to generate biphasic Janus droplets for scale-up.

Parallelized multiple modular microfluidic reactors have been successfully employed for the continuous generation of polymer particles. However, the interaction between parallel channels can affect the flow conditions in each unit when multiple droplet generators share one inlet. To address this issue, an additional 40 mm-long wavy channel was introduced, resulting in lower C.V. of droplets generated compared to a microreactor with a 6 mm-long straight channel at low flow rates (figure 7(c)) [136]. Moreover, the microreactor with the wavy channel did not exhibit a transition to the jetting regime at an increasing flow rate, unlike the one with a straight channel. During the experiment, the productivity was up to 51.2 $\mathrm{ml{\cdot}h^{-1}}$ and the C.V. was less than 5%.

To achieve the required uniformity in parallelized devices, quasi-2D devices are more suitable. Soft lithography based on PDMS is commonly used for manufacturing parallelized flow-focusing devices with a high throughput of emulsion droplets. However, these devices are limited by operating conditions such as temperature and pressure. Alternatively, a 3D etched silicon wafer with 10 260 generators has been reported to produce polycaprolactone solid microparticles with a C.V. $< 5\%$, capable of operating at high pressure and temperature conditions when the fabrication material is silicon and glass [137].

Compared to the flow-focusing generator, the step-emulsification unit has shown superior droplet formation quality, with droplet size being insensitive to flow rates [138]. Rayleigh-Plateau instability is crucial in droplet formation, making it promising to achieve high-throughput production based on the massive parallelization of multiple nozzles [139]. Currently, step-emulsification devices with various geometries are available, including the terrace, straight-through, rectangular-shaped, and wedge-shaped configurations (figure 8).

In a terrace-type step emulsification device, a terrace is located between the inlet and the cavity [144]. The droplet pinch-off location is on the terrace, which promotes pinch-off due to the lower reflux resistance of the continuous phase compared to step emulsification devices without a terrace. Wang *et al* [145] demonstrated a relationship between droplet size and terrace width under conditions where the contact angle is less than 150°. The straight-through type step device is derived from the membrane emulsification device. Asymmetrical channels result in the generation of smaller droplets and improve droplet monodispersity [141]. However, producing droplets with a size of less than 10 μm requires narrower orifices, which leads to the inactivation of most orifices [146].

The research group led by Weitz has extensively investigated different types of step emulsification devices for large-scale droplet generation [142, 143]. A notable example is the millipede device, which utilizes triangular nozzles to generate monodisperse droplets via static instability (figure 8(d)) [143]. At a dripping regime, this device could produce 40 l of droplets with a diameter of 15 μm per hour, whereas the production rate could reach up to 800 l per hour for droplets

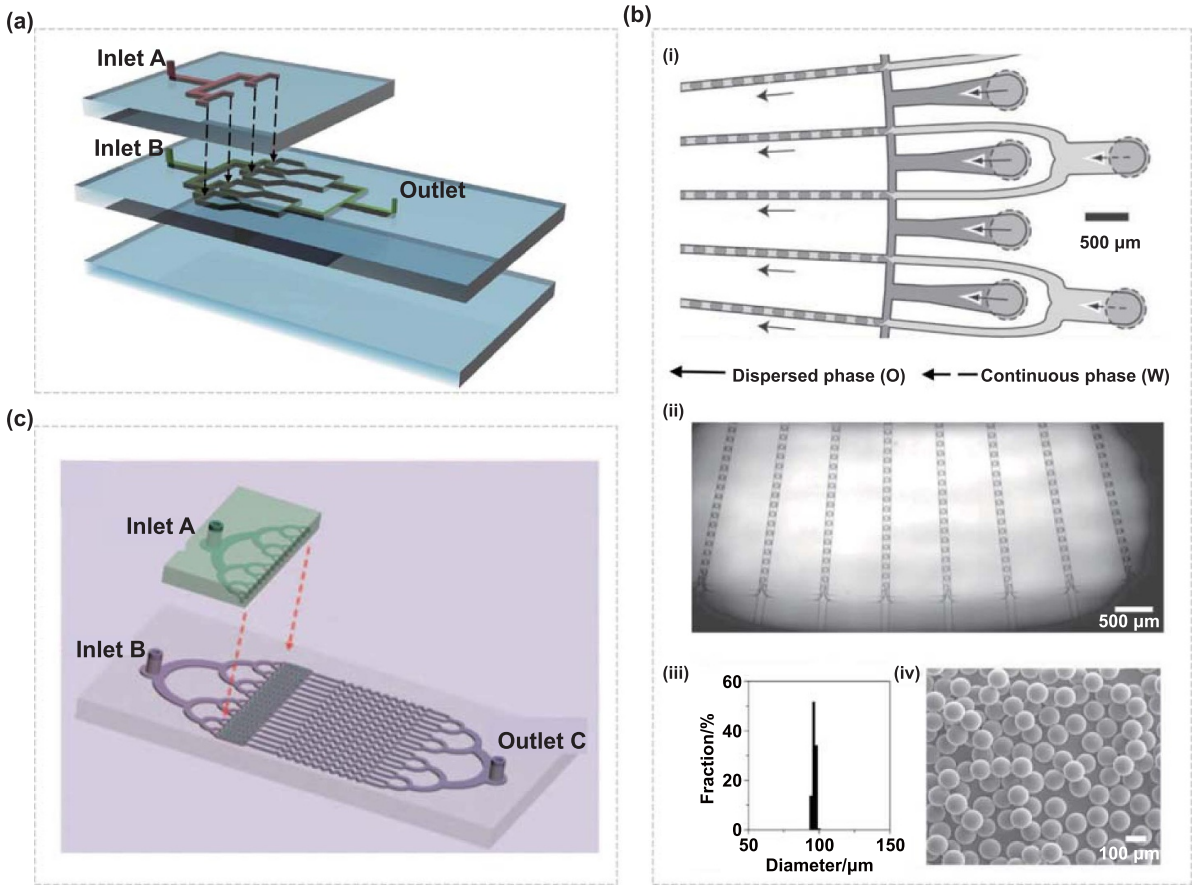

Figure 7. Schematic of parallelization of flow-focusing devices: (a) droplets formed in four integrated flow-focusing devices. Reproduced from [135] with permission from the Royal Society of Chemistry; (b) schematic of planar microfluidic geometries for mass production: (i) magnified view of 128 cross-junctions integrated on a chip, (ii) formation of arrayed monomer droplets (iii) size distribution of the droplets, (iv) SEM image of microspheres. Reproduced from [18] with permission from the Royal Society of Chemistry; (c) a module consisting of 16 individual flow-focusing channels. Reproduced from [136] with permission from the Royal Society of Chemistry.

with a size of around 160 μm. To facilitate the transport of droplets accumulating at the outlet, an open collecting channel along with buoyancy was implemented (figure 8(c)) [142]. This device could generate droplets with a wide range of 30 μm–1 000 μm and a production rate between 0.03 l h^{-1} and 10 l h^{-1}.

In addition to the parallelization of microfluidic droplet generation units, multiple splitting of emulsion droplets is also a viable approach for scale-up. Droplet splitting methods can be classified as active or passive. Passive splitting mechanisms involve breaking up droplets through deliberate fluidic designs, without the need for external forces [20]. This method utilizes microfluidic devices fabricated with high precision to consecutively split monodisperse droplets into smaller ones (figure 9(a)) [129].

The traditional passive splitting with T-junction splits one large droplet into two daughter droplets, while novel multifurcating channels have been developed to enable adjustment of the number and size of daughter droplets [19]. One-to-five splitting microchannels were used to investigate the effect of mother droplet size and channel lengths in the experiment (figure 9(b)), highlighting the versatility of this tool for sample splitting applications [20]. The precision of microfluidic device fabrication was critical, and bypass channels were investigated for bubble splitting [147]. It demonstrated that the C.V. of bubbles generated in the device with bypass channels was significantly smaller than that in the device without bypass channels. For the application of encapsulation of single cells with high throughput, multi-step splitting structures were used to split large droplets into small ones, realizing the droplet generation frequency increasing from 59 Hz to 1 300 Hz (figure 9(c)) [148]. Wu *et al* [149] demonstrated that bifurcating angle of 90° was beneficial for droplet splitting in the fractal tree-shaped network. The effect of capillary number was explored for the droplet size distribution.

4.2. Double emulsion droplets

4.2.1. Conventional microfluidic generation of double emulsion droplets. Double emulsion droplets, which consist of three immiscible phases and exhibit diverse inner structures and morphologies, are the cornerstone of fine emulsion production technology [150, 151]. This technology shows great

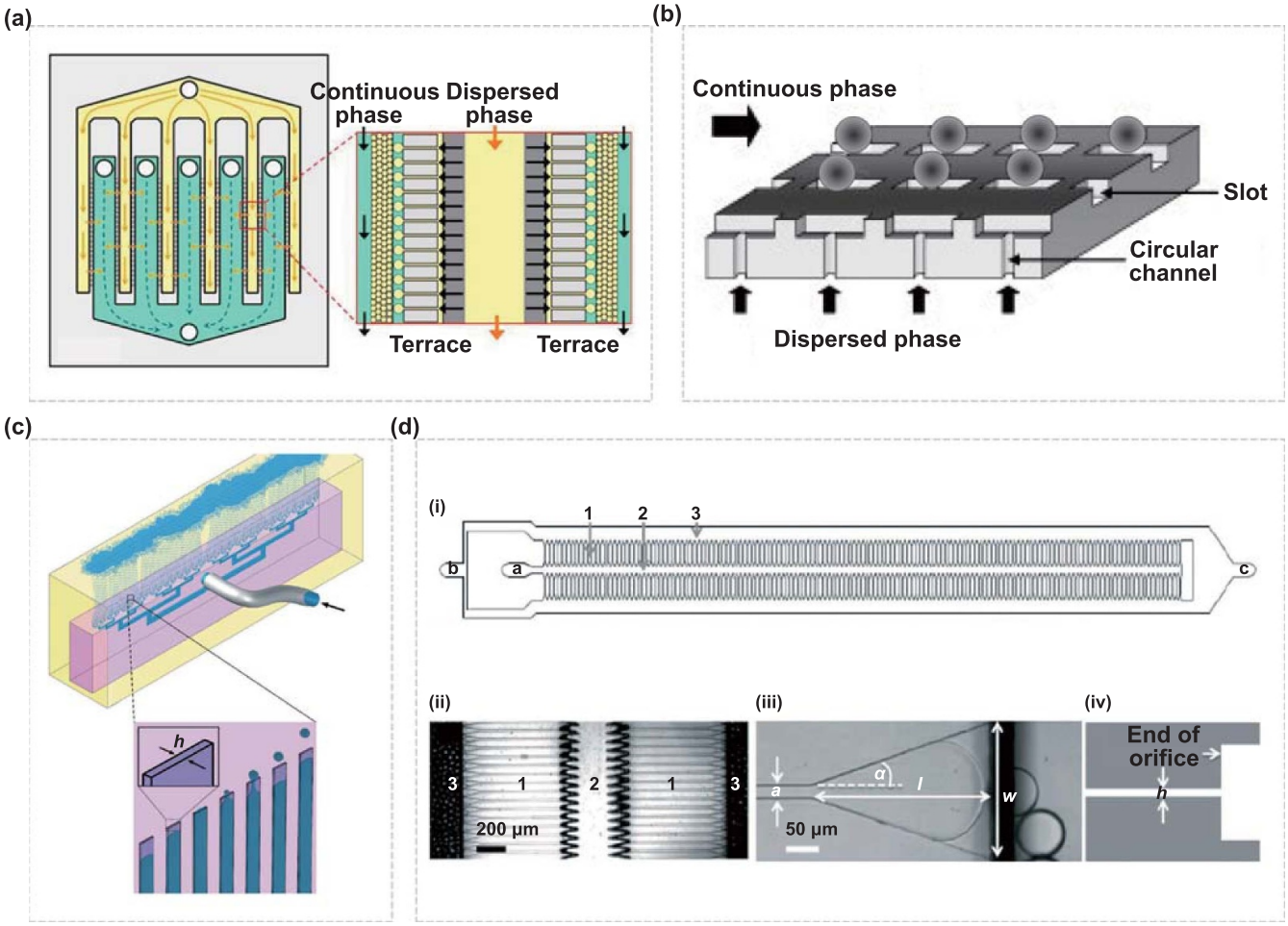

Figure 8. Schematic of parallelization of step-emulsification devices: (a) terrace step-emulsification device. Reprinted from [140], © 2017 Elsevier B.V. All rights reserved; (b) straight-through step emulsification device. Reprinted from [141], Copyright © 2007 Elsevier B.V. All rights reserved; (c) rectangular-shaped step emulsification device. Reproduced from [142] with permission from the Royal Society of Chemistry and (d) wedge-shaped step emulsification devices: (i) schematic illustration of wedge-shaped step emulsification device, (ii) optical micrograph of a section, (iii) optical micrograph of a nozzle, (iv) cross-section of a nozzle. Reproduced from [143] with permission from the Royal Society of Chemistry.

potential for manufacturing highly structured materials for various industrial applications [152]. Therefore, it is crucial to develop precise methods for generating double emulsion droplets [153].

Double emulsion droplets can be generated by microfluidics through the combination of the above single-phase droplet generators in a one-step or two-step process. For example, double emulsion droplets are generated by tandem co-flow and flow-focusing devices in one-step and two-step ways (figure 10). In one-step devices, the inner and middle droplets are simultaneously generated in a coupled co-flow or flow-focusing geometry, forming double emulsion droplets in a single step (figure 10(a)). In two-step devices, the inner-droplets are generated in the first-level co-flow or flow-focusing geometry, then encapsulated by the middle phase downstream into a double emulsion droplet in the second-level geometry (figures 10(b)–(d)). Compared with two-step devices, the one-step devices have lower requirements for channel wall wettability modification due to the consistent encapsulation of the inner phase and are particularly suitable for generating double emulsion droplets with ultra-thin shells [153]. Note that, flow-focusing, co-flow, and cross-junction microfluidic geometries are feasible for generating double emulsion droplets in either one-step or two-step ways, while T-junction and step-emulsification geometries only allow for two-step generation of double emulsion droplets in most flow conditions due to the characteristics of the geometry of the device (figures 10(e)–(h)).

4.2.2. High-throughput microfluidic generation of double emulsion droplets. The strategies for generating high-throughput double emulsion droplets are similar to those for single-phase droplets, involving the parallelization of microfluidic droplet generation units and multiple splitting of emulsion droplets. The appropriate parallelization units for double emulsion droplet generation include flow-focusing generators and step-emulsification units.

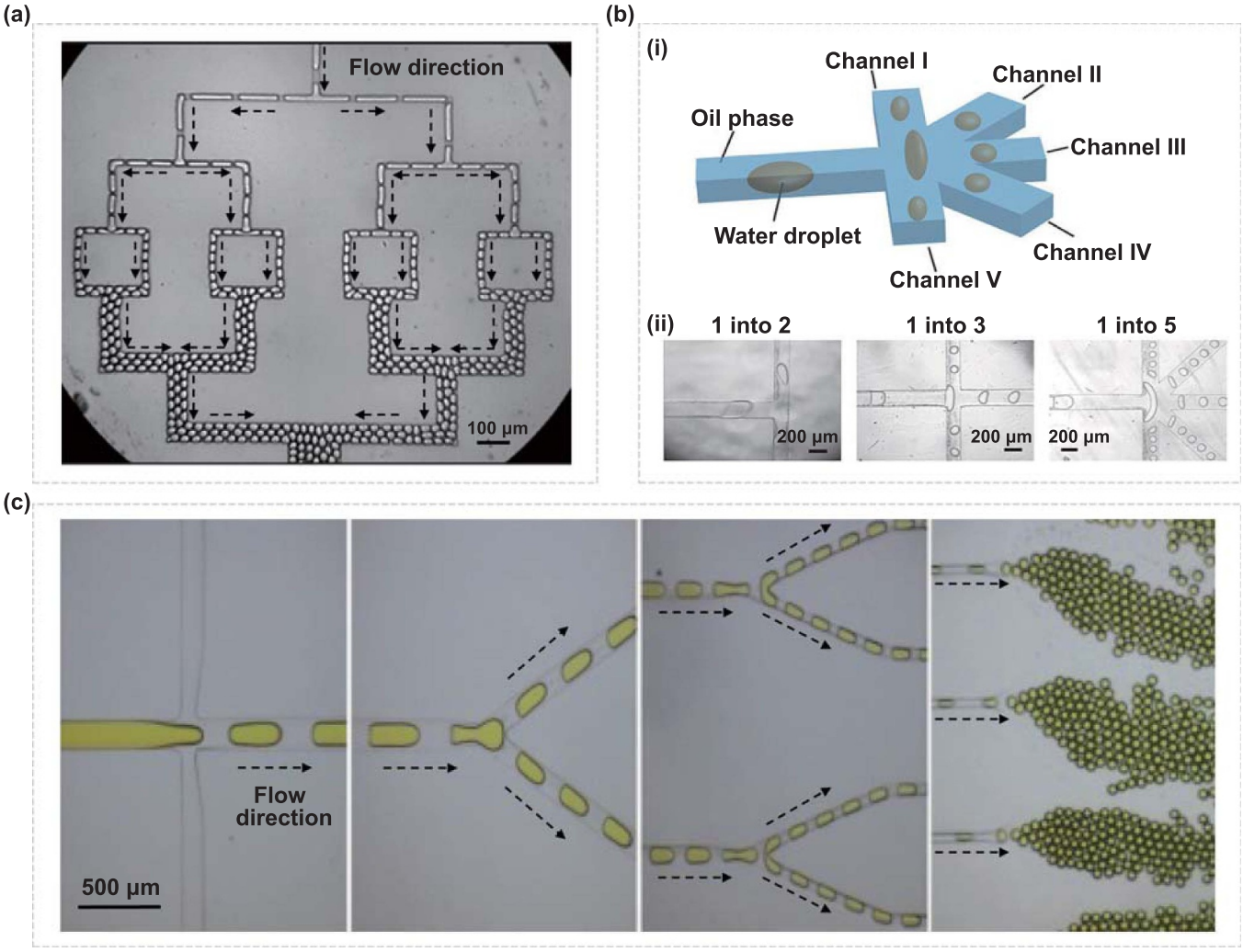

Figure 9. Schematic of multiple splitting of emulsion droplets: (a) droplets formed at high dispersed phase volume fractions. Reprinted figure with permission from [129], Copyright (2004) by the American Physical Society; (b) multiple splitting of droplets with multi-furcating microfluidic channels: (i) droplets splitting set up, (ii) droplets split into two, three, and five daughter droplets. Reprinted from [20], with the permission of AIP Publishing; (c) droplets consecutive splitting via multiple junctions. Reprinted from [148], Copyright © 2015 Zhang-Run Xu. Published by Elsevier B.V. All rights reserved.

The double emulsion droplets generated in the coaxial annular microfluidic platform are a two-step method using parallel flow-focusing generators. As shown in figure 11(a), the inner droplet in the upstream annular channel was emulsified in the downstream cross-junction to form double emulsion droplets. It is applicable for high throughput and controllable production of single and double-emulsified droplets. The annular channels were used to distribute fluids into the droplet-forming units [154]. When Q_i was 5 ml h^{-1}, Q_m was 20 ml h^{-1}, and Q_o was 500 ml h^{-1}, respectively, the core and shell droplet sizes were 88.7 μm and 147.2 μm, respectively, with C.V.s of 5.7% and 2%. 3D distributors and collection channels were used to connect the repeating droplet generators, which enable precise control and mass production of the microfluidic double emulsion droplets. The inner droplets were immediately wrapped by the intermediate fluid at the moment of generation and emulsified into double emulsion droplets, which is a one-step method to generate double emulsion droplets as mentioned above. The device contained 15 droplet-forming units and was connected by three 3D networks of distribution networks and a collection network (figure 11(b)). It demonstrated that this device was capable of producing double emulsion droplets with a C.V. of less than 6% at a rate of 1 kg d^{-1} in a precisely controllable manner [155].

Although parallelized flow-focusing devices have been widely used for emulsion droplet generation, they may suffer from potential issues such as channel clogging or pressure fluctuation, which can result in deteriorated formation processes and polydispersed droplets. It is worth noting that monodispersed emulsions can be generated in step emulsification devices under steady-state conditions. In particular, tandem step emulsification devices have been fabricated to produce monodispersed double emulsion droplets, and the effects of geometrical factors on their morphology, dimensions, and structures have been investigated (figure 12) [63].

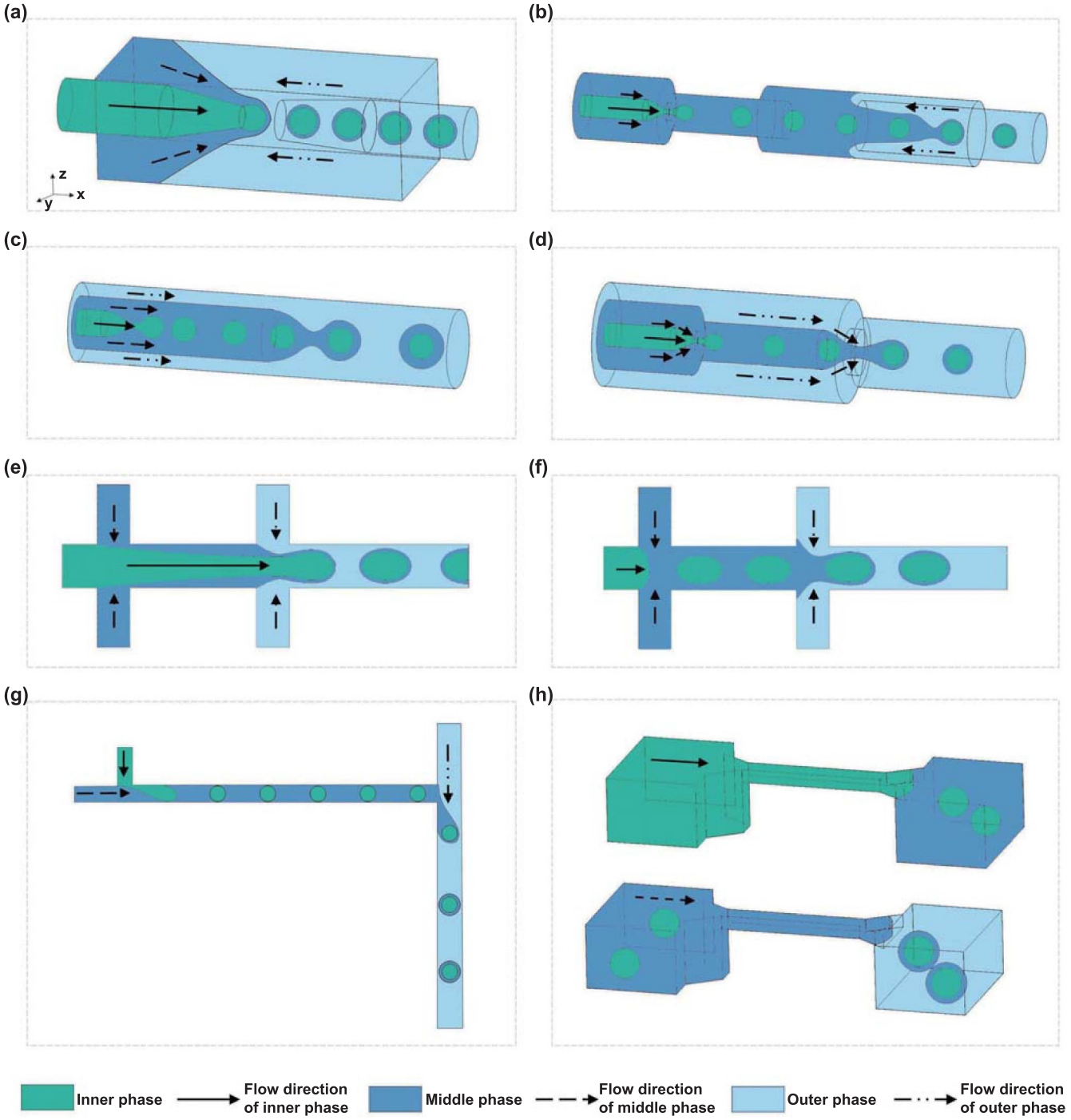

Figure 10. The flow conditions of three phases in (a) one-step co-flow and flow-focusing device, (b) two-step co-flow and flow-focusing device, (c) two-step co-flow device, (d) two-step flow-focusing device, (e) one-step cross-junction device, (f) two-step cross-junction device, (g) two-step T-junction device, (h) two-step step-emulsification device to generate compound droplets.

By adjusting the ratio of the diameters of droplets formed at the end of the first and second-step emulsification nozzles (d_1 and d_2, respectively), various double emulsion droplets with thin-shell, thick-shell, and multicore architectures could be produced. The d_1/d_2 ratio was related to the step heights ratio in the devices. Tandem emulsification has also been applied in millipede devices, where the droplet diameter and core size are related to the channel height [156]. Millipede droplet makers, featuring 200 nozzles in a circular array, could generate 80 drops per second, achieving a production rate of 20 ml·h^{-1}.

Parallelizing the synthesis of double emulsion droplets presents a significant challenge due to the complexity of the required device and the high degree of uniformity needed in manufacturing. One alternative way to realize the high throughput is by splitting large droplets into smaller ones. As

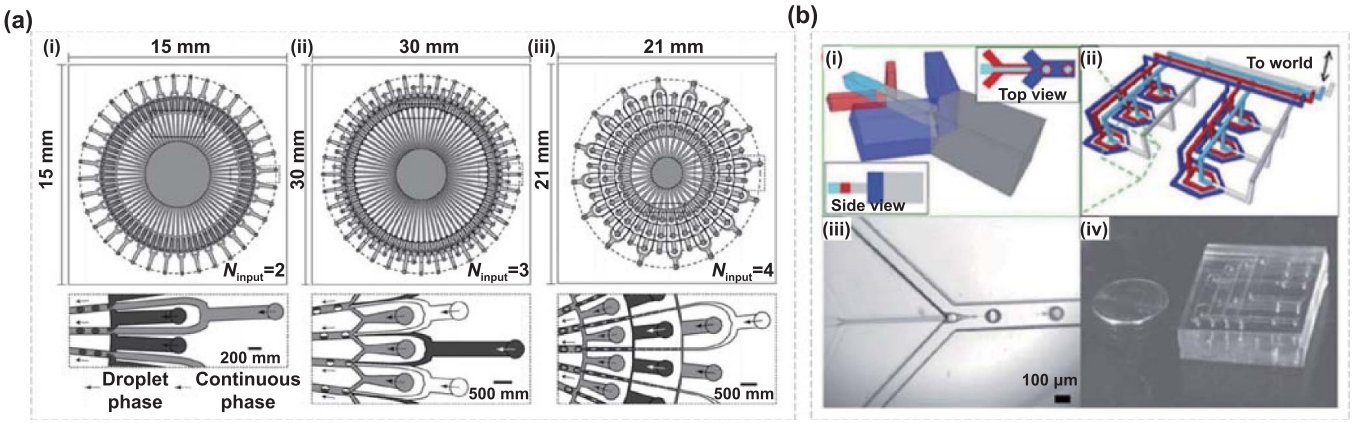

Figure 11. Schematic illustrations of (a) microfluidic chips with annular channels: (i) 144 cross-flow junctions, (ii) 72 droplet generators to produce Janus droplets, (iii) 32 triple emulsion droplet generators. Reproduced from [154] with permission from the Royal Society of Chemistry; (b) schematic of the design for microfluidic double emulsification device: (i) a microfluidic double emulsion droplets-maker unit, (ii) parallelized double emulsion chip, (iii) micrograph of a unit, (iv) actual device. Reproduced from [155] with permission from the Royal Society of Chemistry.

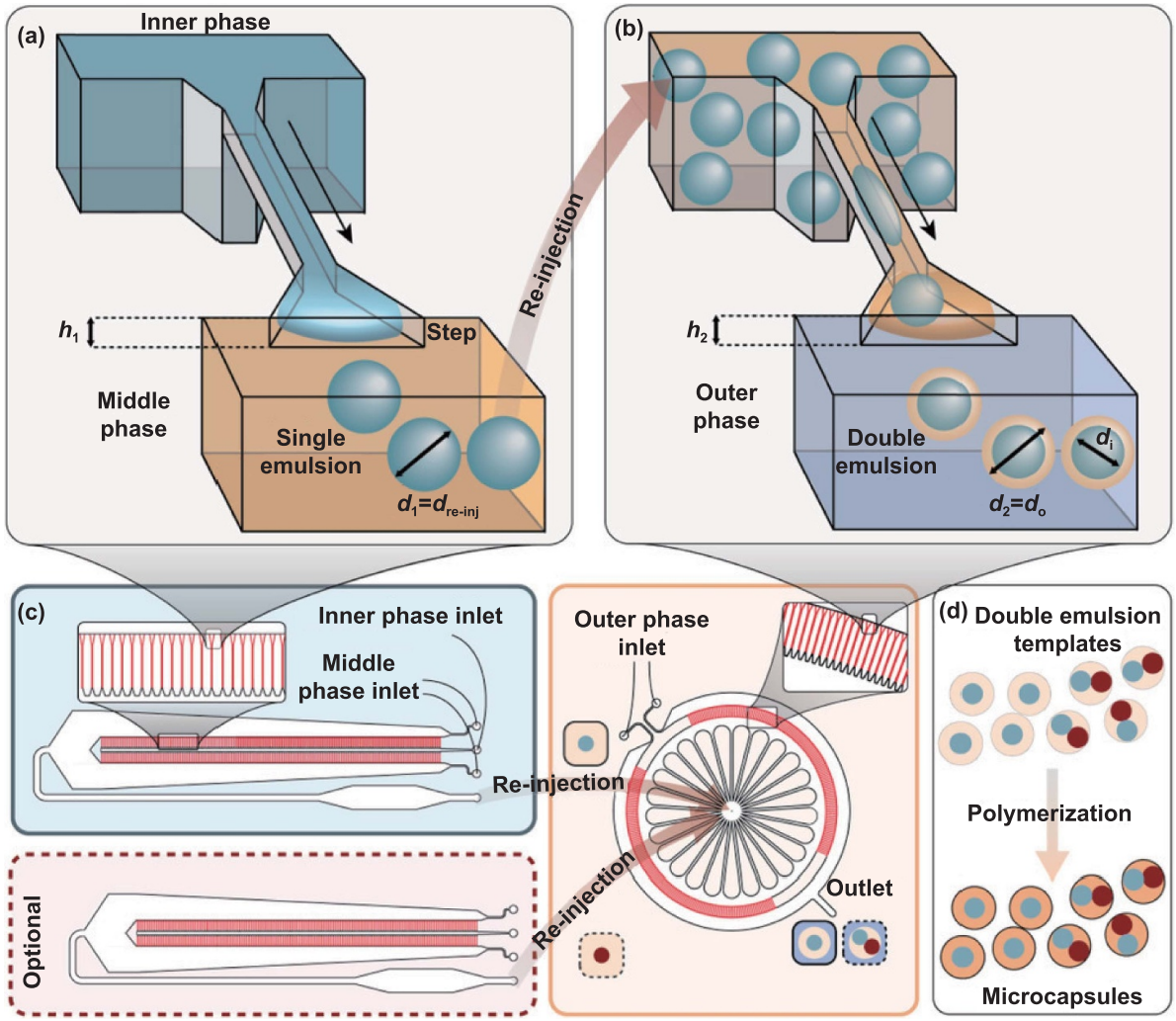

Figure 12. Parallelized step emulsification in tandem glass microfluidic devices: (a) the first step emulsification device, (b) the second step emulsification device, (c) parallelized droplet makers and tandem arrangement of step emulsification device, (d) microcapsules created by polymerizing double emulsion droplets. [63] John Wiley & Sons.© 2018 WILEY-VCH Verlag GmbH & Co. KGaA, Weinheim.

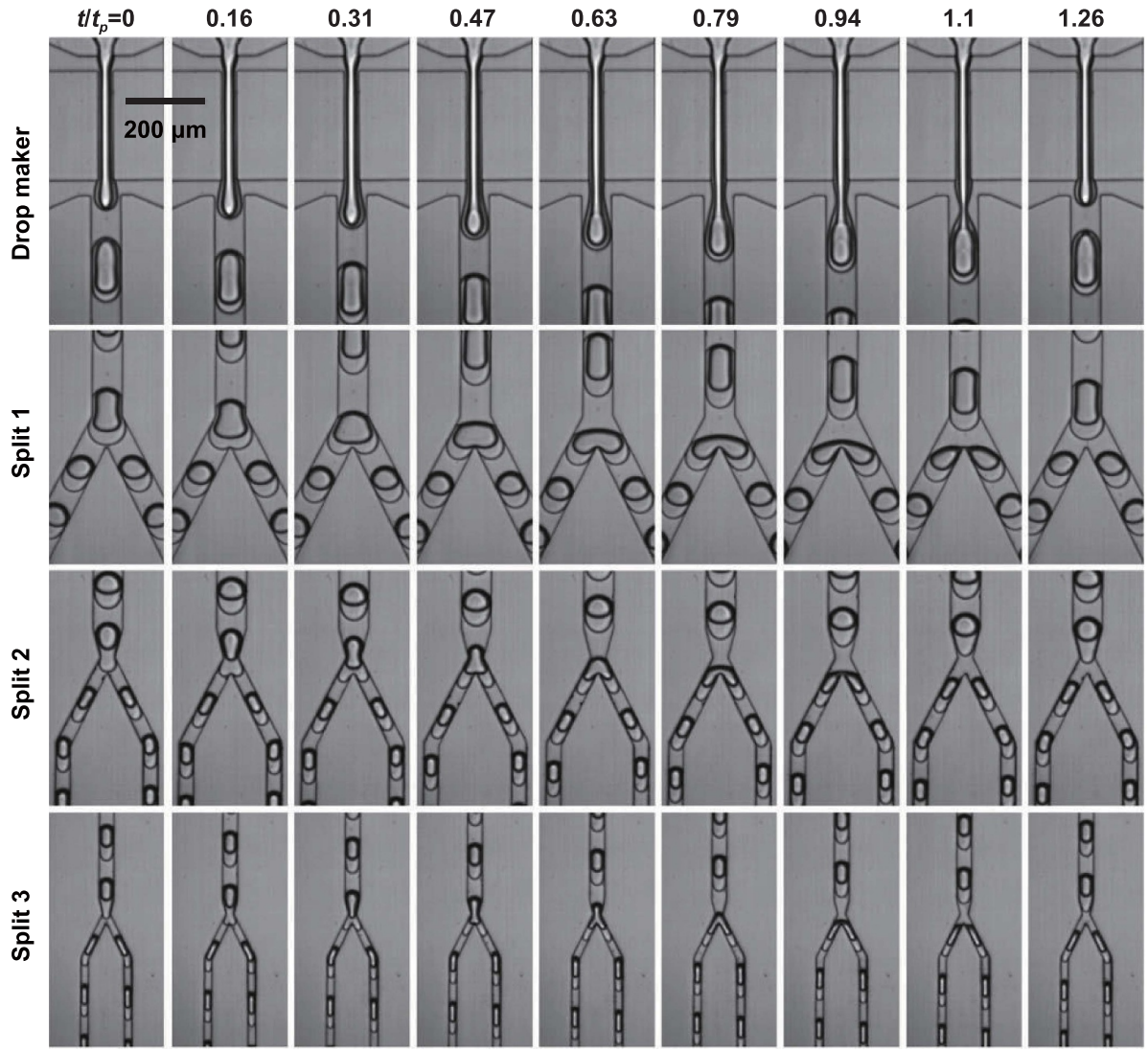

Figure 13. Splitting three times in the emulsion device. Reproduced from [19] with permission from the Royal Society of Chemistry.

shown in figure 13, one double emulsion droplet was split three times into eight identical, smaller drops, increasing throughput by three times. Unlike the usual two-step process, the inner droplets' breakup in this one-step pinching is driven by the outer droplets [19].

Currently, devices for high-throughput double emulsion droplet generation are not widely available, and step emulsion or flow-focusing devices are commonly used in parallelized microfluidic droplet generators. Consistent droplet generator manufacturing is essential to produce high-quality, monodisperse droplets. In parallelized flow-focusing devices, the outer and middle phase flow is regulated to control double emulsion droplet generation methods, whether it is a one-step or two-step process. The two-step method is more commonly used in parallelized step emulsion devices. Additionally, bifurcation structures and size optimization are investigated for multiple droplet splitting. The symmetric breakup of double emulsion droplets in the bifurcation ensures monodispersity. The comparisons between of double emulsion droplets using high-throughput microfluidic production methods are listed in table 3. However, some challenges remain unresolved in microfluidics for droplet generation as mentioned above. Concerning the single-phase droplet generation process, the relationship between microfluidic step emulsification with different device structures and the size of generated droplets remains uncertain, necessitating further investigation through extensive experiments. Additionally, the inherent hydrodynamics of microfluidic step emulsification with different device structures introduce uncertainties that hinder the exploration of high-throughput production. Regarding the double emulsion droplets generation process, one-step microfluidic step emulsification requires higher precision in manufacturing due to the consecutive step structures. On the other hand, the two-step method for generating double emulsion droplets relies on the cooperation among multiple syringe pumps, which makes it time-consuming to explore the suitable flow rates. In summary, future studies should delve deeper into the experiments of microfluidics for droplet generation processes to address these challenges effectively.

Table 3. The comparisons of double emulsion droplets using high-throughput microfluidic production methods.

Method	Qualities					Applicability	References
	Core size	Shell size	C.V. (core)	C.V. (shell)	Yield		
Two-step method using parallel flow-focusing generators	88.7 μm	147.2 μm	5.7%	2.0%	—	Applied to the scale-up production of single-phase droplets, Janus droplets, double emulsion droplets and triple droplets.	[154]
One-step method using parallel flow-focusing generators	104.2 μm	140.3 μm	5.7%	4.1%	>30 tons per year	Applied to the scale-up for the manufacture of precision particles and capsules at the commodity scale.	[155]
Two-step method using parallel flow-focusing generators	64 μm–87 μm	90 μm	—	—	60 ml·h^{-1}	Applied for the scaled-up production of complex emulsions with well-controlled structural parameters	[156]
Two-step method using millipede device	64–87 μm	90 μm	—	—	20 ml·h^{-1}	Applied for the scaled-up production of complex emulsions with well-controlled structural parameters	[156]
Two-step method using millipede device	30 μm	70 μm	—	—	50 ml h^{-1}	Applied for the high-throughput encapsulation of a wide variety of chemicals while providing the exquisite control achievable through microfluidics.	[63]
Multiple splitting	28 μm	43 μm	6%	6%	5 × faster than a conventional drop maker	Applied for the production of small double emulsion droplets.	[19]

4.3. Influencing factors for microfluidic droplet generation

Overall, the size, productivity and composition of the single-phase droplets are manipulated by the following influenced parameters. For the generation of single-phase droplet, the flow rates of continuous phase and dispersed phase are vital in shear-based microfluidic geometries. In the shear-based microfluidic geometries, droplet size decreases with the increasing flow rate of continuous phase, which leads to an increment in the viscous shear and squeezing action. The increase in the dispersed phase flow rate results in the large front of the droplet head and larger pressure inside the droplet, leading to the increment of droplet size [119]. However, the variations of droplet size with dispersed phase flow rate may be different because of the viscosities of dispersed phase and continuous phase [98]. For now, the droplet size prediction in shear-based microfluidic geometries is mainly based on the balance between viscous and interfacial tension forces, while in microfluidic step emulsification device, interfacial tension plays a dominant role [157]. Therefore, droplets formation process in the microfluidic step emulsification device is mainly influenced by the wall wetting effects, so that the microfluidic device channel structure and contact angle of the fluid on the channel wall play a crucial role in the droplet size [158].

Compared with single-phase droplets, three phases are involved in the generation of double emulsion droplets. Hence, the parameters metioned above need to consider the properties of three phases. For instances, the success rate for encapsulation of double emulsion droplets, the cores number, and the droplet size is determined by the synthetically regulation of flow rates of three phases [100]. Similarly, the generation of double emulsion droplets is effected by viscous and interfacial tension forces, so that the size of double emulsion droplets increases with viscosity ratio of middle phase and outer phase [100].

On the other hand, it is worth noting that some non-Newtonian fluids are usually used to produce the microcapsules via the droplet microfluidic method [159], which do not follow Newton's law of viscosity and have variable viscosity dependent on stress [160]. As mentioned above, fluid viscosity is a typical influencing factor to determine the characteristic parameters of the microfluidic droplets generation. Therefore, non-Newtonian fluids effects have also received attention in the microfluidic droplets generation. For examples, it has proved that elasticity of the non-Newtonian dispersed phase is able to extend the thin thread neck of the dispersed phase during the droplet formation in a microfluidic T-junction device. As a result, the generation of droplet will be delayed or even

resisted when compared with the Nowtonian fluids [161]. In addition, with the increasing *We*, the non-Newtonian rheology changes the neck geometry in the jet regime, leading to the increment of generated satellite droplets. Hence, the generated droplets with non-Newtonian fluids are polydispersed and smaller on average compared with those generated with Newtonian fluids [162]. In general, although non-Newtonian fluids effects have been demonstrated to have a non-negligible influence on the performance of the microfluidic droplets generation, there is still a long way to systematically clarify this influence for the decision-making of droplets and the consequent microcapsules.

5. Applications of droplet microfluidics for carbon capture

The core-shell structure is a fundamental morphological characteristic of the microcapsule, which can encapsulate either a single core or multiple cores, referred to as mononuclear or polynuclear, respectively. Highly permeable microencapsulated carbon sorbents have been developed for carbon capture applications (figure 14). Compared to neat liquid sorbents, the mass transfer from the shell is only slightly lower, but the absorption rate is increased by an order-of-magnitude due to the enhancement of the surface area [25]. Fixed bed and fluidized bed are the most commonly used reactor configurations in gas-solid reactions. Therefore, high-throughput generation of microcapsules is employed for industrial scale-up under operating conditions.

5.1. Ionic liquid microcapsules

ILs are a class of organic salts that exist in liquid form at room temperature. Their low vapor pressure and high thermal stability make them highly attractive to carbon capture applications. However, their high viscosity and sensitivity to water have limited their large-scale utilization. Encapsulation of ILs in the microcapsule is an efficient method to address these challenges, as the ILs can be effectively confined with loading efficiencies exceeding 80% and their performance can be significantly improved in the applications of CO_2 handling, microreactors, and heavy metal extraction (figure 15(a)) [163].

Compared with the neat ILs, the properties, including CO_2 solubility, CO_2 sorption, CO_2 selectivity, recycling capacity and regeneration, of encapsulated ILs are enhanced. With the increasing surface area of encapsulated ILs, the solubility of ILs increases. What's more, the viscosity of the IL was reduced due to the use of encapsulated ILs, which improves the CO_2 solubility. Hiraga *et al* [166] have demonstrated that the CO_2 solubility is enhanced due to a coactive effect existing between the molecular interaction and the ILs. It is effective to investigate the adsorption isotherm of microcapsules so as to evaluate absorption performance. Lemusa *et al* [167] reported that high CO_2 solubility of encapsulated ILs is related to the lowest temperature, which is the main factor influencing the CO_2 solubility. In addition, Kaviani *et al* [168] developed a single-step non-solvent induced phase separation method to produce microcapsules, resulting in higher specific surface area and improved absorption rate and CO_2 solubility. It was noted that CO_2 sorption process is evaluated by kinetics and described by the pseudo-second-order model. The encapsulated ILs used in fixed bed absorption were able to overcome the mass transfer restriction of physical absorption. Wang *et al* [169] investigated the sorption kinetic performance of encapsulated ILs in carbon capture, proving that the sorption rate of IL microcapsules is much faster than neat ILs. In-depth investigations into the mass transfer mechanism of encapsulated ILs lead to the development of a kinetic model for CO_2 uptake. Remarkably, the CO_2 capture kinetics of encapsulated ILs exhibit a 50-fold increase compared to the neat liquid [170].

High CO_2 selectivity is a worldwide research topic on exploration of solvents and materials for carbon capture. It was proven that CO_2 selectivity is higher with the increasing IL content in the microcapsules. Mohamed *et al* [171] investigated the selectivity performance through encapsulated ILs and computational study. The results indicated that CO_2 selectivity increases with the high IL content in the zeolitic imidazolate framework-8 (ZIF-8). Furthermore, the effect of viscosity and the mechanism of CO_2/CH_4 selectivity using encapsulated ILs was investigated by the calculations and simulations. In terms of recycling capacity of encapsulated ILs, it is meaningful to check the compatibility and reversibility [172]. For instance, Song *et al* [165] demonstrated that the encapsulated ILs and phase-change ionic liquids (PCILs) have higher CO_2 capacities and superior stability compared to free ILs or PCILs (figure 15(a)). Similarly, Santiago *et al* [164] focused on the potential of encapsulated amino-acid-based ILs (aa-ILs) in CO_2 capture, given their low cost, abundant availability, and non-toxic biodegradability. Encapsulated aa-ILs exhibited high CO_2 absorption capacities and rates, making them promising materials for future CO_2 capture applications (figure 15(b)). Notably, the capture-desorption of CO_2 cycles is accomplished without a significant decrease in successive productivity. Infrared analysis revealed enhanced CO_2 sorption capacity and CO_2/N_2 selectivity of the encapsulated ILs. However, it is observed that the capacity slightly reduced by about 0.104 wt% after eight recycling cycles [173]. Besides, the CO_2 absorption capacity grows up to a certain value and then declines with the increasing recyclability cycles [172]. Stolaroff *et al* [33] produced microcapsules using three promising solvent/shell pairs with a microfluidic flow-focusing capillary device, demonstrating a 3.5-fold enhancement in CO_2 absorption rate compared to the liquid film of the solvent (figure 15(c)). Lemus *et al* [167] conducted a study on the CO_2 absorption of encapsulated ILs at 0.1 MPa and 303 K, reporting a CO_2 absorption capacity of 0.036 g g^{-1} IL. The modest conditions were suitable for the regeneration of encapsulated ILs, and it turned out that the successive capture-desorption CO_2 cycles are obtained without operation productivity loss. Furthermore, the regeneration of ILs is easy because of the low regeneration energy requirement [167]. It is worth noting that, in recent research, various IL materials have been encapsulated

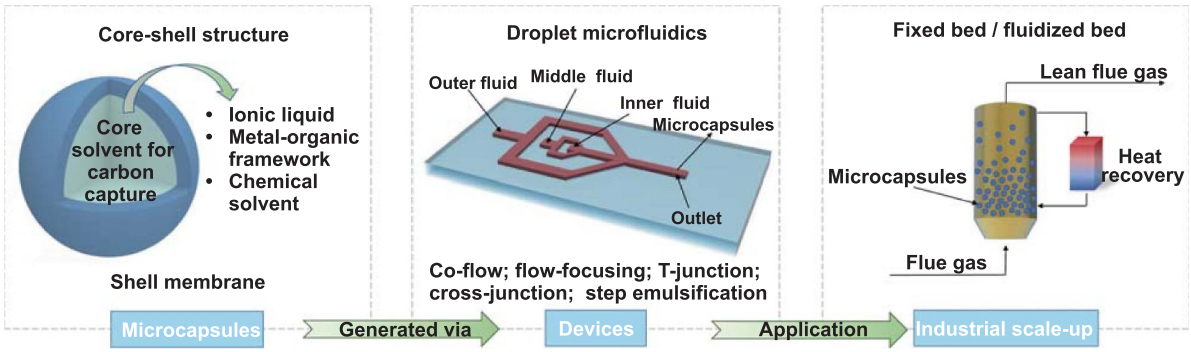

Figure 14. Microcapsules for carbon capture.

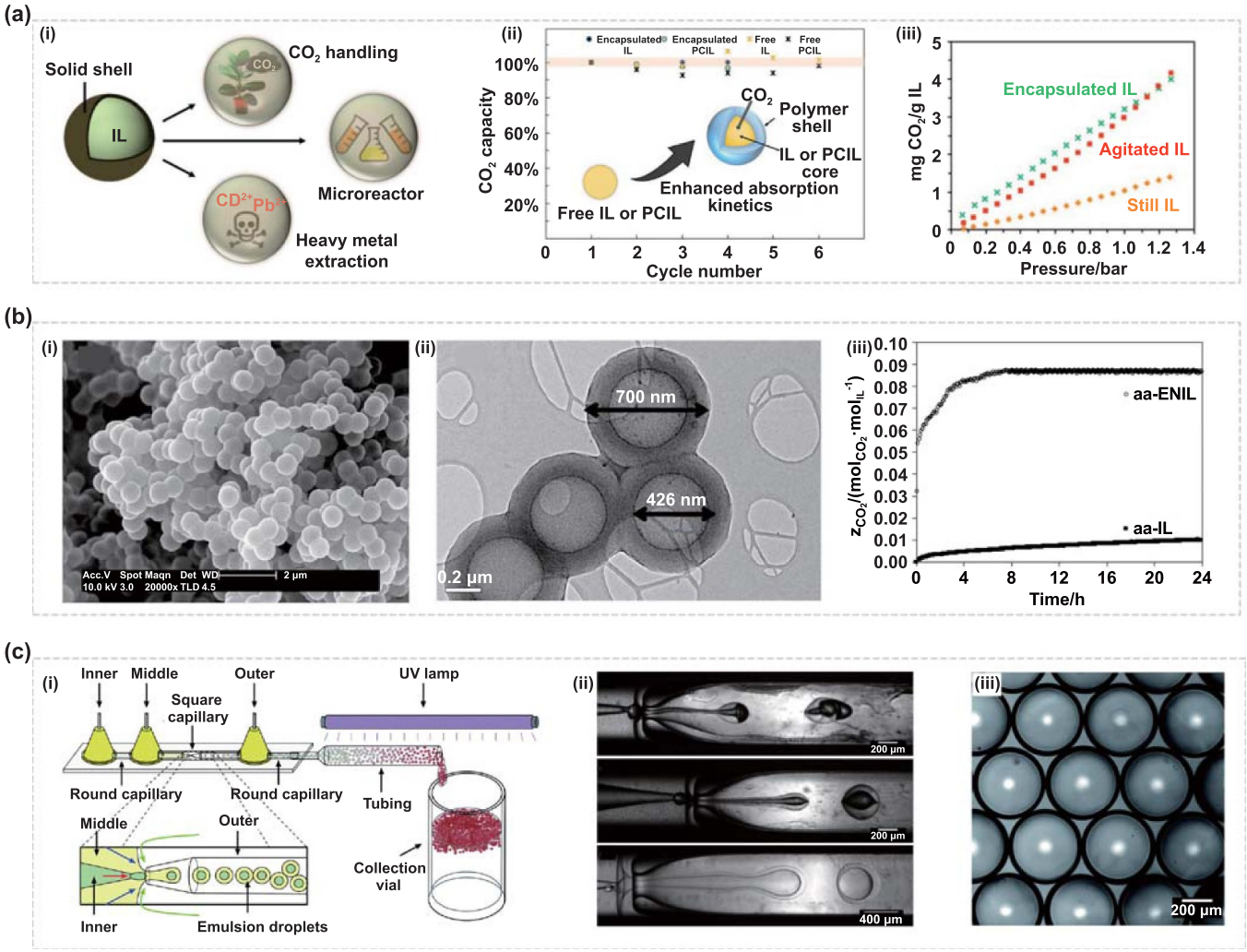

Figure 15. Encapsulate ILs with droplet microfluidics: (a) encapsulation of ILs: (i) multiple advanced applications of encapsulate ILs, (ii) the improvement of CO_2 capacity, (iii) comparison of CO_2 uptake capacity between encapsulated IL, agitated IL, and still IL. Reprinted with permission from [163]. Copyright (2020) American Chemical Society. Reprinted with permission from [164]. Copyright (2018) American Chemical Society; (b) encapsulation of aa-ILs: (i) SEM and (ii) TEM images of the carbon capsules to obtain aa-ILs, (iii) the improvement of CO_2 uptake in aa-ENIL compared to neat aa-ILs. Reprinted with permission from [165]. Copyright (2019) American Chemical Society; (c) schematic of the microfluidic device for encapsulation of ILs: (i) microcapsules generated via the microfluidic flow-focusing device, (ii) the droplet formation process, (iii) micrograph of generated microcapsules. Reproduced from [33] with permission from the Royal Society of Chemistry.

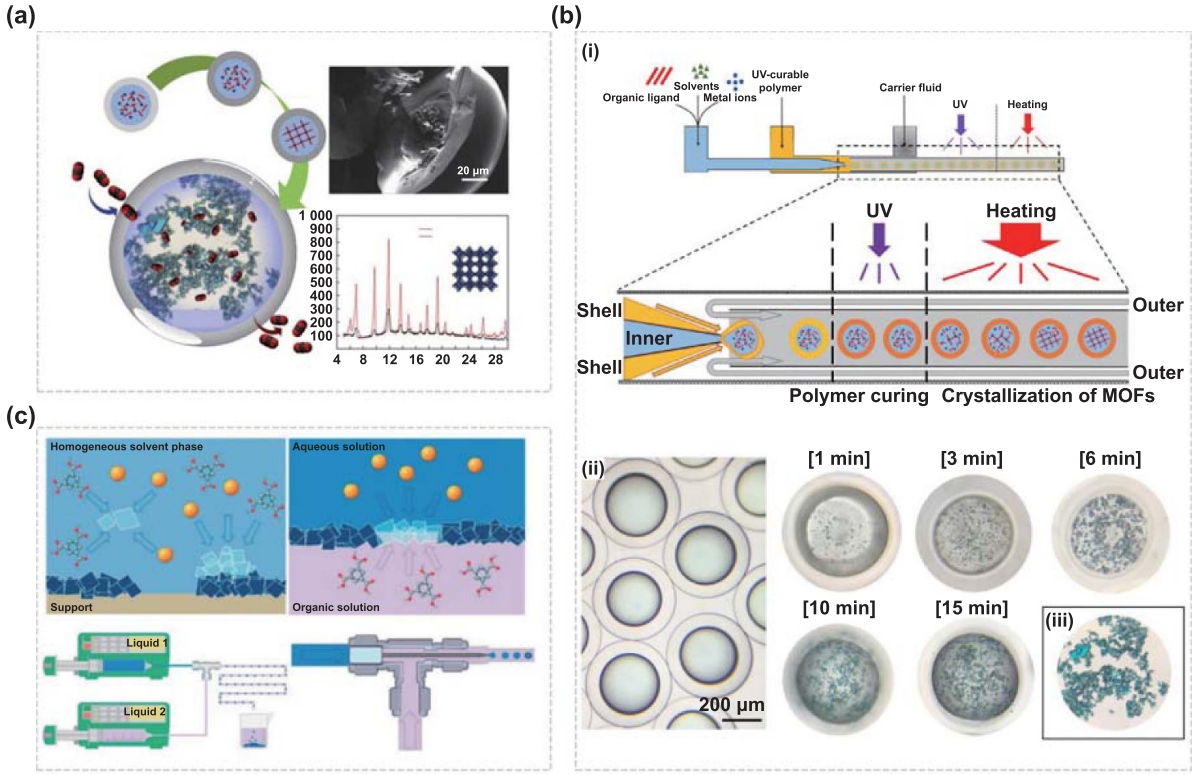

Figure 16. Encapsulate MOFs with droplet microfluidics: (a) the concept of encapsulating MOFs. Reprinted from [14], © 2021 Institute of Process Engineering, Chinese Academy of Sciences. Publishing services by Elsevier B.V. on behalf of KeAi Communications Co., Ltd; (b) encapsulation of MOFs with microfluidic flow-focusing device: (i) schematic of the microfluidic system for encapsulated synthesis of MOFs, (ii) micrograph of generated microcapsules via microfluidics, (iii) micrograph of generated microcapsules via the conventional method. Reprinted from [14], © 2021 Institute of Process Engineering, Chinese Academy of Sciences. Publishing services by Elsevier B.V. on behalf of KeAi Communications Co., Ltd; (c) the concepts in the synthesis of MOF films and preparation of hollow capsules. Adapted from [182], with permission from Springer Nature.

for carbon capture applications, opening up new avenues for improving the efficiency and sustainability of carbon capture technologies [15, 174–176].

5.2. MOF microcapsules

The MOFs are highly porous materials with a large specific surface area, formed by the coordination of metal clusters with organic ligands [177]. Due to their high capture capacity and selectivity, MOFs have become a popular choice for CO_2 capture applications (figure 16(a)). For now, there have been some researches devoted to the fabrication of hollow structured MOF materials. For instance, Zhang *et al* [178] investigated a hollow structured zeolitic imidazolate framework (ZIF-8-H) nanosphere. It proved that the capacity of ZIF-8-H is favorable for binding various sized substrates and it can be recovered and reused without loss of catalytic activity. Furthermore, spray-drying is a versatile method to assemble nanoMOFs into spherical hollow structures [179]. Besides, most MOF adsorption mechanisms are based on physical adsorption, MOF synthesis is a time-consuming process and not easily scalable for large-scale production [180]. To overcome this challenge, a novel MOF-based hybrid sorbent was developed and encapsulated within a glass capillary device (figure 16(b)) [14]. These microcapsules exhibit good recyclability and stability, opening up a new approach for the research of controlled hybrid sorbents. For instance, Hsieh *et al* [181] quantitatively studied the effects of ligand concentration, synthesis time, and temperature on MOF synthesis, which could be beneficial for the development of MOF-based CO_2 capture applications. Additionally, Ameloot *et al* [182] investigated the selective permeability of MOF layers in the shape of hollow microcapsules, and found that the micropore size of MOF crystallites was related to their selective permeability (figure 16(c)). These hollow MOF capsules were generated in a co-flowing stream and it was found that the monodispersity of the generated microcapsules was critical to their performance. Microcapsules encapsulating MOFs exhibit small sizes, facilitating minimum defects and maximum interfacial area for efficient carbon capture. Yu *et al* [14] studied the synthesis of a novel MOF-based hybrid sorbent, wherein they investigated the characteristics of microcapsules containing MOFs for carbon capture applicaitons. By employing a microfluidic strategy, a series of MOFs with hierarchial hollow structures were successfully generated with tunable sizes [183].

The characteristics, including CO_2 uptake, CO_2 selectivity, adsorption capacity, are used to evaluate the performance of MOFs microcapsules on carbon capture. The selectivity of

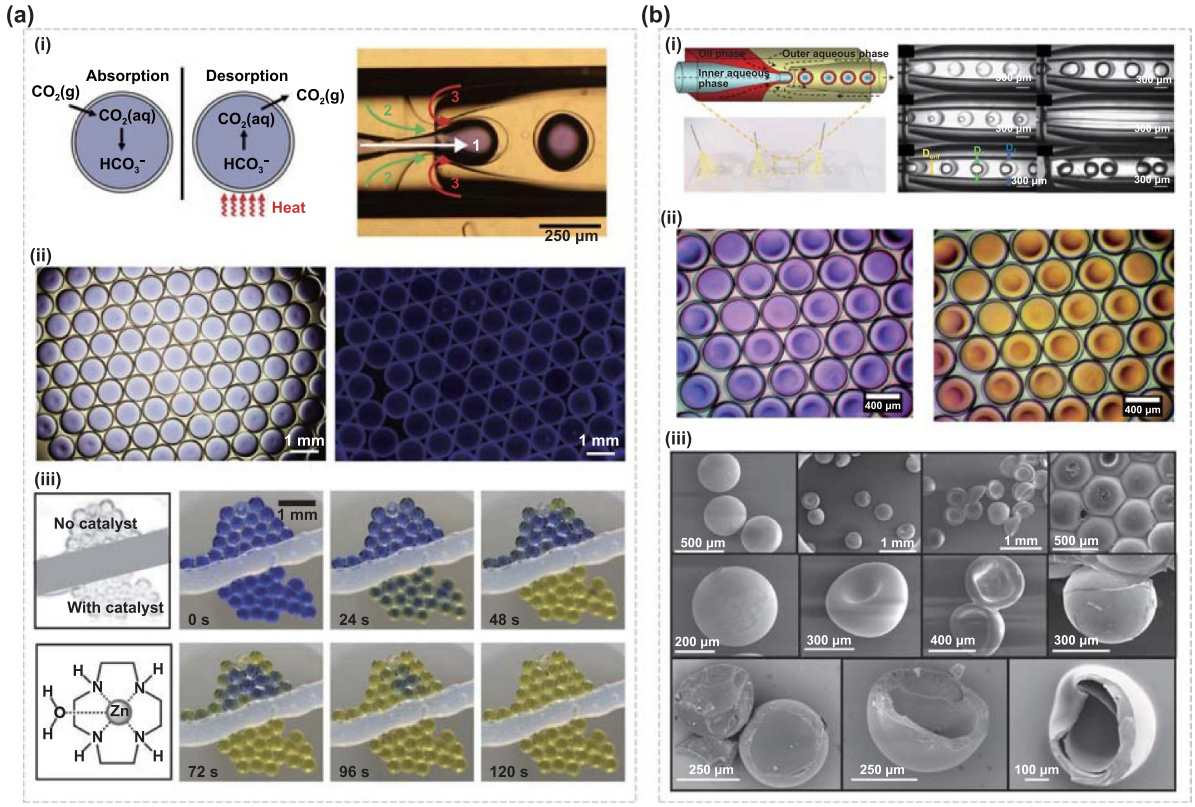

Figure 17. Encapsulate chemical solvents with droplet microfluidics: (a) encapsulation of chemical solvents for carbon capture: (i) schematic illustration of the encapsulated liquid carbon capture process via the microfluidic flow-focusing device, (ii) optical image of cured silicon microcapsules, (iii) optical images of microcapsules in flowing CO_2 environment. Reproduced from [25], with permission from Springer Nature; (b) encapsulation of K_2CO_3 for carbon capture: (i) schematic illustration of the encapsulated K_2CO_3 via the microfluidic flow-focusing device, (ii) the color change of microcapsules before and after carbon capture, (iii) SEM images of capsules within different shell materials. [13] John Wiley & Sons.© 2022 Wiley Periodicals LLC.

CO_2/CH_4 separation was improved by functionalizing MOFs with amino groups [184]. The equilibrium selectivity for selective adsorption of CO_2 over CH_4 can be over 10 based on the MOFs with various unsaturated sites [185]. The commercially available $Cu_3(BTC)_2$ MOF showed a selectivity of $4 \sim 6$ at $0.1 \sim 3$ bar [186]. Compared with a silica with high surface area, a MOF replete with open magnesium site has an exceptional adsorption capacity up to 23.6 wt% CO_2 at 0.1 bar and 296 K [187]. Among all the commercial adsorbents, zeolite 13X is the most effective adsorbent for CO_2 separation [53]. Compared with zeolite 13X, the adsorption capacities are higher in a magnesium-based MOF [51]. Furthermore, various sites, such as open metal sites and Lewis basic sites, are introduced into MOFs to improve the adsorption capacity. Liang *et al* [45] synthesized a Cu-MOF with high CO_2 uptake and selectivity, which is able to be reused without loss of adsorption capacity. The results demonstrated that these microcapsules achieved higher efficiency and catalyst recyclability, presenting a promising avenue for future applications in assembling MOFs with novel hierarchical structures.

5.3. Chemical solvent encapsulation

Chemical absorbents, such as ethanolamine (MEA), piperazine, and carbonate solutions, have been encapsulated for carbon capture. Encapsulation of these absorbents in microcapsules has been shown to increase the uptake rate of CO_2 and mass transfer when compared with the use of neat fluid [188, 189]. It is worth noting that, MEA, which is most used in a number of plants, is corrosive and it will degrade during repeated regeneration cycles [190]. Hence, relying on the characteristics of abundance and eco-friendly, carbonate solutions are studied as an alternative to MEA solutions in carbon capture. For instance, Vericella *et al* [25] employed a core-shell motif to encapsulate potassium carbonate (K_2CO_3) or sodium carbonate (Na_2CO_3) (figure 17(a)). The microcapsules demonstrated higher permeability than gas separation membranes, and the CO_2 absorption rate was increased by an order of magnitude. The process of CO_2 absorption-desorption could be visually monitored with a pH indicator. It turned out that the CO_2 sorption capacity of encapsulated sodium carbonate is similar to that of MEA. Zhao *et al* [13] produced stable microcapsules with CO_2 solvents using flow-focusing microfluidics (figure 17(b)). These microcapsules withstand temperatures up to 300 °C and could be used for multiple regeneration cycles. Wang *et al* [191] utilized a 3D flow-focusing microfluidic device to produce microcapsules for carbon capture, in which nanoparticle organic hybrid materials were encapsulated. The CO_2 capture rate was enhanced due to the specific surface area and enhanced mass transfer of

Table 4. The comparisons of performance parameters of carbon capture microcapsules fabricated via the droplet microfluidics method.

Size	Core material	Shell material	Stability	CO_2 uptake rate	CO_2 adsorption	Number of cycles	References
(900 ± 100) nm	1-ethyl-3-methylimadazolium bis(trifluoromethylsulfonyl) Imide	Acetone	448 (475) °C	—	—	4	[167]
(900 ± 100) nm	N-methyl-2-hydroxyethylammonium pentanoate	Acetone	140 (205 °C	—	—	4	[167]
1 ∼ 2 mm	1-ethyl-3-methylimidazolium bis(trifluoromethylsulfonyl)imide	Polymeric	—	—	3 mol CO_2·kg^{-1} IL	10	[168]
1 ∼ 2 mm	1-hexyl-3-methylimidazolium bis(trifluoromethylsulfonyl) imide	Polymeric	—	—	2.4 mol CO_2·kg^{-1} IL	10	[168]
430 μm	NOHM-I-PEI	Silicone acrylate	—	3–4 orders of magnitude greater	3 mol CO_2·kg^{-1} IL	—	[170]
100–600 μm	$[P_{2228}][2CNPyr]$	PDMS polymer	—	—	0.6 ∼ 0.9 mol CO_2·mol^{-1} IL	7	[165]
100–600 μm	$[P_{2222}][BnIm]$	PDMS polymer	—	—	0.6 ∼ 0.9 mol CO_2 ·mol^{-1} IL (60 °C) 0.6 ∼ 0.85 mol CO_2 ·mol^{-1} IL (70 °C) 0.3 ∼ 0.8 mol CO_2 ·mol^{-1} IL (80 °C)	6	[165]
700 nm	1-butyl-3-methylimidazolium prolinate	aluminosilicate	520 K	0.53 (303 K, 20 bar)	0.038 g CO_2·g^{-1} IL (303 K)	—	[164]
700 nm	1-butyl-3-methylimidazolium methioninate	aluminosilicate	513 K	0.52 (303 K, 20 bar)	0.031 g CO_2·g^{-1} IL (303 K)	—	[164]
700 nm	1-butyl-3-methylimidazolium glycinate	aluminosilicate	500 K	0.50 (303 K, 20 bar)	0.020 g CO_2·g^{-1} IL (303 K)	—	[164]
400 μm	precursors of HKUST-1	TEGO RAD 2 650	—	—	4 mmol CO_2·g^{-1} MOF	10	[14]
(600 ± 6) μm	aqueous carbonate solution	Semicosil 949UV	—	—	7.1% g CO_2·g^{-1} sodium carbonate	> 80	[25]
360 ∼ 510 μm	K_2CO_3	1,6-hexanediol diacrylate	—	—	0.003 ∼ 1.82 mmol CO_2·g^{-1} K_2CO_3	—	[13]
300 μm	NOHMs solvent	Semicosil 949UV	—	—	—	—	[191]
2.5 ∼ 10 μm	$KHCO_3$	Hydrochar	—	—	2.50 ∼ 4.26 mmol·g^{-1}	—	[192]

microcapsules. Additionally, Shi *et al* [192] utilized $KHCO_3$ as the form of carbon spheres for CO_2 capture, which exhibited superior CO_2 capture performance with a CO_2 uptake of up to 4.26 mmol·g^{-1} at 25 °C and 1 bar. Rama *et al* [193] used 2-amino-2-methyl-1-propanol (AMP) as the core sorbent in microcapsules, demonstrating its high CO_2 sorption capacity and its potential applicability in industrial settings. Finn and Galvin [194] proposed a mechanistic model for mass transfer and chemical reaction to predict microcapsule performance under different scenarios. The model's predictions indicated that microcapsules containing sodium carbonate solution show strong sensitivity and high CO_2 sorption capacity. The comparisons of performance parameters of carbon capture microcapsules fabricated via the droplet microfluidics method are listed in table 4.

6. Conclusions and perspectives

The increasing emission of CO_2 from various sources is drawing attention toward CCUS strategies. Therefore, it is promising to explore the generation of carbon capture microcapsules via droplet microfluidics. This review has provided a comprehensive overview of the progress and limitations of the high-throughput production of carbon capture microcapsules by microfluidics. The advancements in microfluidic device fabrication, methods and hydrodynamics for droplet generation, and the application of high-throughput emulsion for carbon capture have been discussed. The main fabrication methods of microfluidic devices are wet etching using glass/silicon substrates, soft lithography using PDMS, hot embossing on PMMA, capillary assembly, and 3D printing technology. The methods and hydrodynamics of co-flow, T-junction, cross-junction, and flow-focusing microfluidic droplets generation have been studied in depth, including flow modes transition and monodispersity of droplets in dripping mode. In addition, the hydrodynamics of step emulsification for droplet generation have been demonstrated to have a close association with the device geometries. This fundamental understanding of the hydrodynamics of the microfluidic droplet generation process is helpful for high-throughput droplet generation. The review emphasizes the importance of both parallelized microfluidic droplet generators and multiple splitting of droplet approaches for achieving high-throughput production.

In the recent years, the carbon capture microcapsules generated via droplet microfluidics have aroused considerable interset. However, there remain challenges and opportunities to address for the future applications. Therefore, herein, the most prominent research directions for microcapsules for carbon capture based on the droplet microfluidics are provided on three significant aspects: (i) high-throughput production of microcapsules; (ii) selectivity of materials for carbon capture microcapsules; (iii) quality of microcapsules.

6.1. High-throughput production of microcapsules

Generally, microcapsules are synthesized using interfacial polycondensation or photocuring droplets. As the templates of microcapsules, double emulsion droplets generated from microfluidic devices are monodispersed, controllable and concentricity, which are superior to those generated with bulk emulsification. Although plenty of microencapsulated carbon sorbents via droplet microfluidics have been proven to be effective for the carbon capture applications, the output of microcapsules is not enough to satisfy the industrial application. In order to increase the throughput of microcapsules based on the droplet microfluidics, parallelization of microfluidic droplet generation units and multiple splitting of emulsion droplets are effective. However, considering various materials can be applied for carbon capture, the fabrication factors of microfluidic devices for high-throughput microfluidic production of the microcapsules, such as cost, manipulation, and stability, are taken into account. In general, until now, the relevant researches involving the high-throughput production of microcapsules for carbon capture have not been really started yet.

6.2. Selectivity of materials for carbon capture microcapsules

The materials selectivity of shell and core of microcapsules is essential for the applications of carbon capture. The shell of microcapsules presents a primary protective function against environments. Furthermore, selective permeability, waterproofing and biocompatibility of the shell are also needed to be considered. The core of microcapsules is the essential element because of its key role to make carbon capture functional in the application, and it will be isolated from the external agents. Focusing on the application of carbon capture, the ideal chemical solvents enclosed into the microcapsules require the following characteristics: (i) high reactivity to CO_2; (ii) low regeneration cost requirements; (iii) high absorption capacity; (iv) high thermal stability; (v) reduced solvent degradation; (vi) low environmental impact; (vii) low solvent costs. For now, ILs, MOFs and chemical solvent have been selected as the core materials. It is meaningful to explore other materials, whose absorption kinetics will be increased due to the encapsulation or the inherent characteristics such as corrosive or highly viscous. The permeability of CO_2 through the cured shell material is also needed to be taken into account so that the microcapsules can be used in cycles.

6.3. Quality of microcapsules

In order to evaluate the quality of microcapsules, the numbers of C.V., shell diameter, and core diameter are used and illustrated in the available researches. For examples, Vericella *et al* [25] generated microcapsules with a highly uniform diameter of (600 $\pm$ 6) μm, wall thickness of (31 $\pm$ 1) μm and centricity. Wang *et al* [173] generated spherical microcapsules with diameter of 38 μm. Yew *et al* [195] produced functional core-shell microcapsules of uniform sizes with 600–720 μm, and the C.V. with 0.97% $\sim$ 3%. Especially, the monodispersity and centricity of microcapsules are demonstrated to be beneficial for the increment of surface area. However, the relationship between the quality of microcapsules and the CO_2 absorption

properties has been far from being fully understood. It is also wondering that whether the size of microcapsules will influence the CO_2 absorption properties.

This review can trigger novel ideas for other applications such as high-throughput generation of microcapsules for carbon capture, which is beneficial for the application of microfluidic droplet technology, particularly in the industrial fields. In the future, one challenge in mass production is the design regulations and tactics for non-Newtonian fluid. The embodiment of quality control in parallelized droplet generators for the long-term future also needs to be investigated further. In conclusion, the generation of high-throughput droplets is an important link between theoretical research and industrial applications.

Acknowledgments

This work was supported by the National Natural Science Foundation of China (No. 52036006).

ORCID iD

Yongping Chen https://orcid.org/0000-0003-3927-3797

References

[1] Lashof D A and Ahuja D R 1990 Relative contributions of greenhouse gas emissions to global warming *Nature* **344** 529–31
[2] Centi G and Perathoner S 2009 Opportunities and prospects in the chemical recycling of carbon dioxide to fuels *Catal. Today* **148** 191–205
[3] Olah G A, Goeppert A and Prakash G K S 2009 Chemical recycling of carbon dioxide to methanol and dimethyl ether: from greenhouse gas to renewable, environmentally carbon neutral fuels and synthetic hydrocarbons *J. Org. Chem.* **74** 487–98
[4] Sakakura T, Choi J C and Yasuda H 2007 Transformation of carbon dioxide *Chem. Rev.* **107** 2365–87
[5] Gao W L *et al* 2020 Industrial carbon dioxide capture and utilization: state of the art and future challenges *Chem. Soc. Rev.* **49** 8584–686
[6] Arneth A *et al* 2017 Historical carbon dioxide emissions caused by land-use changes are possibly larger than assumed *Nat. Geosci.* **10** 79–84
[7] Yaacob N F F, Mat Yazid M R, Abdul Maulud K N and Ahmad Basri N E 2020 A review of the measurement method, analysis and implementation policy of carbon dioxide emission from transportation *Sustainability* **12** 5873
[8] Mukherjee A, Dhiman V K, Srivastava P and Kumar A 2021 Intellectual tool to compute embodied energy and carbon dioxide emission for building construction materials *J. Phys.: Conf. Ser.* **1950** 012025
[9] Cox P M, Betts R A, Jones C D, Spall S A and Totterdell I J 2000 Acceleration of global warming due to carbon-cycle feedbacks in a coupled climate model *Nature* **408** 184–7
[10] Jiang K, Ashworth P, Zhang S Y, Liang X, Sun Y and Angus D 2020 China's carbon capture, utilization and storage (CCUS) policy: a critical review *Renew. Sustain. Energy Rev.* **119** 109601
[11] Ma Q M and Xu J H 2023 Green microfluidics in microchemical engineering for carbon neutrality *Chin. J. Chem. Eng.* **53** 332–45
[12] Li L R, Zhang C B, Chen Y P and Liu X D 2022 The use of nanoparticles for high-efficiency CO_2 capture by methanol *J. CO_2 Util.* **66** 102299
[13] Zhao Y, Moshtaghibana S, Zhu T L, Fayemiwo K A, Price A and Vladisavljević G T 2022 Microfluidic fabrication of novel polymeric core-shell microcapsules for storage of CO_2 solvents and organic chelating agents *J. Polym. Sci.* **60** 1727–40
[14] Yu W, Gao M, Rim G, Feric T G, Rivers M L, Alahmed A, Jamal A and Park A H A 2021 Novel in-capsule synthesis of metal–organic framework for innovative carbon dioxide capture system *Green Energy Environ.* **8** 767–74
[15] Lee Y Y, Edgehouse K, Klemm A, Mao H C, Pentzer E and Gurkan B 2020 Capsules of reactive ionic liquids for selective capture of carbon dioxide at low concentrations *ACS Appl. Mater. Interfaces* **12** 19184–93
[16] Tetradis-Meris G, Rossetti D, De Torres C P, Cao R, Lian G P and Janes R 2009 Novel parallel integration of microfluidic device network for emulsion formation *Ind. Eng. Chem. Res.* **48** 8881–9
[17] Kobayashi I, Wada Y, Uemura K and Nakajima M 2010 Microchannel emulsification for mass production of uniform fine droplets: integration of microchannel arrays on a chip *Microfluid. Nanofluidics* **8** 255–62
[18] Nisisako T and Torii T 2008 Microfluidic large-scale integration on a chip for mass production of monodisperse droplets and particles *Lab Chip* **8** 287–93
[19] Abate A R and Weitz D A 2011 Faster multiple emulsification with drop splitting *Lab Chip* **11** 1911–5
[20] Li Z D, Li L Q, Liao M X, He L Q and Wu P 2019 Multiple splitting of droplets using multi-furcating microfluidic channels *Biomicrofluidics* **13** 024112
[21] Hao G Q, Yu C, Chen Y Y, Liu X D and Chen Y P 2022 Controlled microfluidic encapsulation of phase change material for thermo-regulation *Int. J. Heat Mass Transfer* **190** 122738
[22] Liu H and Crooks R M 2011 Three-dimensional paper microfluidic devices assembled using the principles of origami *J. Am. Chem. Soc.* **133** 17564–6
[23] Zhang J L, Liu S X, Yang P Y and Sui G 2011 Rapid detection of algal toxins by microfluidic immunoassay *Lab Chip* **11** 3516–22
[24] Li J, Chen H S and Stone H A 2011 Breakup of double emulsion droplets in a tapered nozzle *Langmuir* **27** 4324–7
[25] Vericella J J *et al* 2015 Encapsulated liquid sorbents for carbon dioxide capture *Nat. Commun.* **6** 6124
[26] Chen C H, Sarkar A, Song Y A, Miller M A, Kim S J, Griffith L G, Lauffenburger D A and Han J 2011 Enhancing protease activity assay in droplet-based microfluidics using a biomolecule concentrator *J. Am. Chem. Soc.* **133** 10368–71
[27] Zhang L, Wang W, Ju X J, Xie R, Liu Z and Chu L Y 2015 Fabrication of glass-based microfluidic devices with dry film photoresists as pattern transfer masks for wet etching *RSC Adv.* **5** 5638–46
[28] Kang X J, Luo C X, Wei Q, Xiong C Y, Chen Q, Chen Y and Ouyang Q 2013 Mass production of highly monodisperse polymeric nanoparticles by parallel flow focusing system *Microfluid. Nanofluidics* **15** 337–45
[29] Kricka L J, Fortina P, Panaro N J, Wilding P, Alonso-Amigo G and Becker H 2002 Fabrication of plastic microchips by hot embossing *Lab Chip* **2** 1–4
[30] Yu Y R, Shang L R, Guo J H, Wang J and Zhao Y J 2018 Design of capillary microfluidics for spinning cell-laden microfibers *Nat. Protocols* **13** 2557–79

[31] Zhang J, Xu W H, Xu F Y, Lu W W, Hu L Y, Zhou J L, Zhang C and Jiang Z 2021 Microfluidic droplet formation in co-flow devices fabricated by micro 3D printing *J. Food Eng.* **290** 110212

[32] Ghaznavi A *et al* 2022 A monolithic 3D printed axisymmetric co-flow single and compound emulsion generator *Micromachines* **13** 188

[33] Stolaroff J K, Ye C W, Oakdale J S, Baker S E, Smith W L, Nguyen D T, Spadaccini C M and Aines R D 2016 Microencapsulation of advanced solvents for carbon capture *Faraday Discuss.* **192** 271–81

[34] Wang C M, Luo X Y, Luo H M, Jiang D E, Li H R and Dai S 2011 Tuning the basicity of ionic liquids for equimolar CO_2 capture *Angew. Chem., Int. Ed.* **50** 4918–22

[35] Cadena C, Anthony J L, Shah J K, Morrow T I, Brennecke J F and Maginn E J 2004 Why is CO_2 so soluble in imidazolium-based ionic liquids? *J. Am. Chem. Soc.* **126** 5300–8

[36] Gurkan B E, de La Fuente J C, Mindrup E M, Ficke L E, Goodrich B F, Price E A, Schneider W F and Brennecke J F 2010 Equimolar CO_2 absorption by anion-functionalized ionic liquids *J. Am. Chem. Soc.* **132** 2116–7

[37] Zhang X P, Zhang X C, Dong H F, Zhao Z J, Zhang S J and Huang Y 2012 Carbon capture with ionic liquids: overview and progress *Energy Environ. Sci.* **5** 6668–81

[38] Shi X Y, Xiao H, Azarabadi H, Song J Z, Wu X L, Chen X and Lackner K S 2020 Sorbents for the direct capture of CO_2 from ambient air *Angew. Chem., Int. Ed.* **59** 6984–7006

[39] Angell C A, Ansari Y and Zhao Z F 2012 Ionic liquids: past, present and future *Faraday Discuss.* **154** 9–27

[40] Liu Y, Sun J H, Huang H H, Bai L L, Zhao X M, Qu B H, Xiong L Q, Bai F Q, Tang J W and Jing L Q 2023 Improving CO_2 photoconversion with ionic liquid and Co single atoms *Nat. Commun.* **14** 1457

[41] Vishwakarma N K, Singh A K, Hwang Y H, Ko D H, Kim J O, Babu A G and Kim D P 2017 Integrated CO_2 capture-fixation chemistry via interfacial ionic liquid catalyst in laminar gas/liquid flow *Nat. Commun.* **8** 14676

[42] Plechkova N V and Seddon K R 2008 Applications of ionic liquids in the chemical industry *Chem. Soc. Rev.* **37** 123–50

[43] Nandi S, De Luna P, Daff T D, Rother J, Liu M, Buchanan W, Hawari A I, Woo T K and Vaidhyanathan R 2015 A single-ligand ultra-microporous MOF for precombustion CO_2 capture and hydrogen purification *Sci. Adv.* **1** e1500421

[44] Kumar A, Madden D G, Lusi M, Chen K J, Daniels E A, Curtin T, Perry J J and Zaworotko M J 2015 Direct air capture of CO_2 by physisorbent materials *Angew. Chem., Int. Ed.* **54** 14372–7

[45] Liang L F, Liu C P, Jiang F L, Chen Q H, Zhang L J, Xue H, Jiang H L, Qian J J, Yuan D Q and Hong M C 2017 Carbon dioxide capture and conversion by an acid-base resistant metal-organic framework *Nat. Commun.* **8** 1233

[46] Sculley J P and Zhou H C 2012 Enhancing amine-supported materials for ambient air capture *Angew. Chem., Int. Ed.* **51** 12660–1

[47] Y M V *et al* 2020 Cooperative carbon dioxide adsorption in alcoholamine- and alkoxyalkylamine-functionalized metal-organic frameworks *Angew. Chem., Int. Ed.* **59** 19468–77

[48] Simmons J M, Wu H, Zhou W and Yildirim T 2011 Carbon capture in metal–organic frameworks—a comparative study *Energy Environ. Sci.* **4** 2177

[49] Aniruddha R, Sreedhar I and Reddy B M 2020 MOFs in carbon capture-past, present and future *J. CO2 Util.* **42** 101297

[50] Saha D, Bao Z B, Jia F and Deng S G 2010 Adsorption of CO_2, CH_4, N_2O, and N_2 on MOF-5, MOF-177, and zeolite 5A *Environ. Sci. Technol.* **44** 1820–6

[51] Bao Z B, Yu L, Ren Q L, Lu X Y and Deng S G 2011 Adsorption of CO_2 and CH_4 on a magnesium-based metal organic framework *J. Colloid Interface Sci.* **353** 549–56

[52] Trickett C A, Helal A, Al-Maythalony B A, Yamani Z H, Cordova K E and Yaghi O M 2017 The chemistry of metal–organic frameworks for CO_2 capture, regeneration and conversion *Nat. Rev. Mater.* **2** 17045

[53] Cavenati S, Grande C A and Rodrigues A E 2004 Adsorption equilibrium of methane, carbon dioxide, and nitrogen on Zeolite 13X at high pressures *J. Chem. Eng. Data* **49** 1095–101

[54] Wang M, Lawal A, Stephenson P, Sidders J and Ramshaw C 2011 Post-combustion CO_2 capture with chemical absorption: a state-of-the-art review *Chem. Eng. Res. Des.* **89** 1609–24

[55] Rubin E S, Mantripragada H, Marks A, Versteeg P and Kitchin J 2012 The outlook for improved carbon capture technology *Prog. Energy Combust. Sci.* **38** 630–71

[56] Liao P Z, Wu X, Wang M H, Li Z M and Qian F 2023 Robust control and flexible operation for commercial-scale coal-fired power plant with solvent-based post-combustion carbon capture *Int. J. Greenhouse Gas Control* **123** 103831

[57] Rubin E S 2008 CO_2 capture and transport *Elements* **4** 311–7

[58] van der Spek M, Arendsen R, Ramirez A and Faaij A 2016 Model development and process simulation of postcombustion carbon capture technology with aqueous AMP/PZ solvent *Int. J. Greenhouse Gas Control* **47** 176–99

[59] Vaidya P D and Kenig E Y 2007 CO_2-alkanolamine reaction kinetics: a review of recent studies *Chem. Eng. Technol.* **30** 1467–74

[60] Kittel J, Idem R, Gelowitz D, Tontiwachwuthikul P, Parrain G and Bonneau A 2009 Corrosion in MEA units for CO_2 capture: pilot plant studies *Energy Proc.* **1** 791–7

[61] Didas S A, Choi S, Chaikittisilp W and Jones C W 2015 Amine-oxide hybrid materials for CO_2 capture from ambient air *Acc. Chem. Res.* **48** 2680–7

[62] Gebald C, Wurzbacher J A, Tingaut P, Zimmermann T and Steinfeld A 2011 Amine-based nanofibrillated cellulose as adsorbent for CO_2 capture from air *Environ. Sci. Technol.* **45** 9101–8

[63] Ofner A, Mattich I, Hagander M, Dutto A, Seybold H, Rühs P A and Studart A R 2019 Controlled massive encapsulation via tandem step emulsification in glass *Adv. Funct. Mater.* **29** 1806821

[64] Zhao Y J, Shum H C, Chen H S, Adams L L A, Gu Z Z and Weitz D A 2011 Microfluidic generation of multifunctional quantum dot barcode particles *J. Am. Chem. Soc.* **133** 8790–3

[65] Kim S H, Shim J W and Yang S M 2011 Microfluidic multicolor encoding of microspheres with nanoscopic surface complexity for multiplex immunoassays *Angew. Chem., Int. Ed.* **50** 1171–4

[66] Anbari A, Chien H T, Datta S S, Deng W, Weitz D A and Fan J 2018 Microfluidic model porous media: fabrication and applications *Small* **14** 1703575

[67] Scott S M and Ali Z 2021 Fabrication methods for microfluidic devices: an overview *Micromachines* **12** 319

[68] Deshmukh S S and Goswami A 2020 Hot embossing of polymers—a review *Mater. Today* **26** 405–14

[69] Datta S, Deshmukh S S, Kar T and Goswami A 2023 A review on modelling and numerical simulation of micro hot embossing process: fabrication, mold filling behavior, and demolding analysis *Eng. Res. Express* **5** 012006

[70] Ge Q, Li Z Q, Wang Z L, Kowsari K, Zhang W, He X N, Zhou J L and Fang N X 2020 Projection micro

stereolithography based 3D printing and its applications *Int. J. Extrem. Manuf.* **2** 022004
[71] Xia Y N and Whitesides G M 1998 Soft lithography *Annu. Rev. Mater. Sci.* **28** 153–84
[72] Makamba H, Kim J H, Lim K, Park N and Hahn J H 2003 Surface modification of poly(dimethylsiloxane) microchannels *Electrophoresis* **24** 3607–19
[73] Jeyhani M, Thevakumaran R, Abbasi N, Hwang D K and Tsai S S H 2020 Microfluidic generation of all-aqueous double and triple emulsions *Small* **16** 1906565
[74] Qin D, Xia Y N and Whitesides G M 1996 Rapid prototyping of complex structures with feature sizes larger than 20 μm *Adv. Mater.* **8** 917–9
[75] Mcdonald J C and Whitesides G M 2002 Poly(dimethylsiloxane) as a material for fabricating microfluidic devices *Acc. Chem. Res.* **35** 491–9
[76] Duffy D C, McDonald J C, Schueller O J A and Whitesides G M 1998 Rapid prototyping of microfluidic systems in poly(dimethylsiloxane) *Anal. Chem.* **70** 4974–84
[77] Shu C S, Su Q T, Li M H, Wang Z B, Yin S H and Huang S 2022 Fabrication of extreme wettability surface for controllable droplet manipulation over a wide temperature range *Int. J. Extrem. Manuf.* **4** 045103
[78] Ali U, Karim K J B A and Buang N A 2015 A review of the properties and applications of poly (methyl methacrylate) (PMMA) *Polym. Rev.* **55** 678–705
[79] Vladisavljević G T, Kobayashi I and Nakajima M 2012 Production of uniform droplets using membrane, microchannel and microfluidic emulsification devices *Microfluid. Nanofluidics* **13** 151–78
[80] Peng L F, Deng Y J, Yi P Y and Lai X M 2014 Micro hot embossing of thermoplastic polymers: a review *J. Micromech. Microeng.* **24** 013001
[81] Chu L Y, Utada A S, Shah R K, Kim J W and Weitz D A 2007 Controllable monodisperse multiple emulsions *Angew. Chem., Int. Ed.* **46** 8970–4
[82] Shah R K *et al* 2008 Designer emulsions using microfluidics *Mater. Today* **11** 18–27
[83] Chen Y P, Liu X D, Zhang C B and Zhao Y J 2015 Enhancing and suppressing effects of an inner droplet on deformation of a double emulsion droplet under shear *Lab Chip* **15** 1255–61
[84] Gross B, Lockwood S Y and Spence D M 2017 Recent advances in analytical chemistry by 3D printing *Anal. Chem.* **89** 57–70
[85] Meng Z J, Mu X D, He J K, Zhang J L, Ling R and Li D C 2023 Embedding aligned nanofibrous architectures within 3D-printed polycaprolactone scaffolds for directed cellular infiltration and tissue regeneration *Int. J. Extrem. Manuf.* **5** 025001
[86] Q Z M *et al* 2023 3D printed fiber-optic nanomechanical bioprobe *Int. J. Extrem. Manuf.* **5** 015005
[87] Ma X L 2013 Research on application of SLA technology in the 3D printing technology *Appl. Mech. Mater.* **401–403** 938–41
[88] Yun J S, Park T W, Jeong Y H and Cho J H 2016 Development of ceramic-reinforced photopolymers for SLA 3D printing technology *Appl. Phys.* A **122** 629
[89] Wu H, Fahy W P, Kim S, Kim H, Zhao N, Pilato L, Kafi A, Bateman S and Koo J H 2020 Recent developments in polymers/polymer nanocomposites for additive manufacturing *Prog. Mater. Sci.* **111** 100638
[90] Revilla-León M and Özcan M 2019 Additive manufacturing technologies used for processing polymers: current status and potential application in prosthetic dentistry *J. Prosthodont.* **28** 146–58
[91] Sui S *et al* 2023 Additive manufacturing of magnesium and its alloys: process-formability-microstructure-performance relationship and underlying mechanism *Int. J. Extrem. Manuf.* **5** 042009
[92] Mu Y B, Chu Y Q, Pan L, Wu B K, Zou L F, He J F, Han M S, Zhao T S and Zeng L 2023 3D printing critical materials for rechargeable batteries: from materials, design and optimization strategies to applications *Int. J. Extrem. Manuf.* **5** 042008
[93] Cramer C, Fischer P and Windhab E J 2004 Drop formation in a co-flowing ambient fluid *Chem. Eng. Sci.* **59** 3045–58
[94] Homma S, Koga J, Matsumoto S, Song M and Tryggvason G 2006 Breakup mode of an axisymmetric liquid jet injected into another immiscible liquid *Chem. Eng. Sci.* **61** 3986–96
[95] Guillot P, Colin A, Utada A S and Ajdari A 2007 Stability of a jet in confined pressure-driven biphasic flows at low reynolds numbers *Phys. Rev. Lett.* **99** 104502
[96] Utada A S, Fernandez-Nieves A, Stone H A and Weitz D A 2007 Dripping to jetting transitions in coflowing liquid streams *Phys. Rev. Lett.* **99** 094502
[97] Utada A S, Fernandez-Nieves A, Gordillo J M and Weitz D A 2008 Absolute instability of a liquid jet in a coflowing stream *Phys. Rev. Lett.* **100** 014502
[98] Castro-Hernández E, Gundabala V, Fernández-Nieves A and Gordillo J M 2009 Scaling the drop size in coflow experiments *New J. Phys.* **11** 075021
[99] Gupta A, Matharoo H S, Makkar D and Kumar R 2014 Droplet formation via squeezing mechanism in a microfluidic flow-focusing device *Comput. Fluids* **100** 218–26
[100] Chen Y P, Wu L Y and Zhang L 2015 Dynamic behaviors of double emulsion formation in a flow-focusing device *Int. J. Heat Mass Transfer* **82** 42–50
[101] Yu W, Li B, Liu X D and Chen Y P 2021 Hydrodynamics of triple emulsion droplet generation in a flow-focusing microfluidic device *Chem. Eng. Sci.* **243** 116648
[102] Engl W, Backov R and Panizza P 2008 Controlled production of emulsions and particles by milli- and microfluidic techniques *Curr. Opin. Colloid Interface Sci.* **13** 206–16
[103] Utada A S, Lorenceau E, Link D R, Kaplan P D, Stone H A and Weitz D A 2005 Monodisperse double emulsions generated from a microcapillary device *Science* **308** 537–41
[104] Chen H S, Li J, Shum H C, Stone H A and Weitz D A 2011 Breakup of double emulsions in constrictions *Soft Matter* **7** 2345
[105] Takeuchi S, Garstecki P, Weibel D B and Whitesides G M 2005 An axisymmetric flow-focusing microfluidic device *Adv. Mater.* **17** 1067–72
[106] Anna S L, Bontoux N and Stone H A 2003 Formation of dispersions using "flow focusing" in microchannels *Appl. Phys. Lett.* **82** 364–6
[107] Cristini V and Tan Y C 2004 Theory and numerical simulation of droplet dynamics in complex flows—a review *Lab Chip* **4** 257–64
[108] Garstecki P, Gitlin I, DiLuzio W, Whitesides G M, Kumacheva E and Stone H A 2004 Formation of monodisperse bubbles in a microfluidic flow-focusing device *Appl. Phys. Lett.* **85** 2649–51
[109] Garstecki P, Stone H A and Whitesides G M 2005 Mechanism for flow-rate controlled breakup in confined geometries: a route to monodisperse emulsions *Phys. Rev. Lett.* **94** 164501
[110] Gañán-Calvo A M, González-Prieto R, Riesco-Chueca P, Herrada M A and Flores-Mosquera M 2007 Focusing capillary jets close to the continuum limit *Nat. Phys.* **3** 737–42
[111] Garstecki P, Fuerstman M J, Stone H A and Whitesides G M 2006 Formation of droplets and bubbles in a microfluidic

T-junction-scaling and mechanism of break-up *Lab Chip* **6** 437–46
[112] De Menech M, Garstecki P, Jousse F and Stone H A 2008 Transition from squeezing to dripping in a microfluidic T-shaped junction *J. Fluid Mech.* **595** 141–61
[113] Lin R, Fisher J S, Simon M G and Lee A P 2012 Novel on-demand droplet generation for selective fluid sample extraction *Biomicrofluidics* **6** 024103
[114] Ding Y, Casadevall I, Solvas X and deMello A 2015 "V-junction": a novel structure for high-speed generation of bespoke droplet flows *Analyst* **140** 414–21
[115] Abate A R, Poitzsch A, Hwang Y, Lee J, Czerwinska J and Weitz D A 2009 Impact of inlet channel geometry on microfluidic drop formation *Phys. Rev.* E **80** 026310
[116] Sontti S G and Atta A 2020 Numerical insights on controlled droplet formation in a microfluidic flow-focusing device *Ind. Eng. Chem. Res.* **59** 3702–16
[117] Yu W, Liu X D, Zhao Y J and Chen Y P 2019 Droplet generation hydrodynamics in the microfluidic cross-junction with different junction angles *Chem. Eng. Sci.* **203** 259–84
[118] Funfschilling D, Debas H, Li H Z and Mason T G 2009 Flow-field dynamics during droplet formation by dripping in hydrodynamic-focusing microfluidics *Phys. Rev.* E **80** 015301
[119] Wu S C, Chen J, Liu X D and Yao F 2021 Experimental study of droplet formation in the cross-junction *J. Dispers. Sci. Technol.* **42** 1233–40
[120] Abate A R and Weitz D A 2009 High-order multiple emulsions formed in poly(dimethylsiloxane) microfluidics *Small* **5** 2030–2
[121] Kendall M R, Bardin D, Shih R, Dayton P A and Lee A P 2012 Scaled-up production of monodisperse, dual layer microbubbles using multi-array microfluidic module for medical imaging and drug delivery *Bubble Sci. Eng. Technol.* **4** 12–20
[122] Yu W, Liu X D, Li B and Chen Y P 2022 Experiment and prediction of droplet formation in microfluidic cross-junctions with different bifurcation angles *Int. J. Multiph. Flow* **149** 103973
[123] Mittal N, Cohen C, Bibette J and Bremond N 2014 Dynamics of step-emulsification: from a single to a collection of emulsion droplet generators *Phys. Fluids* **26** 082109
[124] Montessori A, Lauricella M, Succi S, Stolovicki E and Weitz D 2018 Elucidating the mechanism of step emulsification *Phys. Rev. Fluids* **3** 072202(R)
[125] Sugiura S, Nakajima M, Iwamoto S and Seki M 2001 Interfacial tension driven monodispersed droplet formation from microfabricated channel array *Langmuir* **17** 5562–6
[126] Eggersdorfer M L, Seybold H, Ofner A, Weitz D A and Studart A R 2018 Wetting controls of droplet formation in step emulsification *Proc. Natl Acad. Sci. USA* **115** 9479–84
[127] Mulligan M K and Rothstein J P 2012 Scale-up and control of droplet production in coupled microfluidic flow-focusing geometries *Microfluid. Nanofluidics* **13** 65–73
[128] Barbier V, Willaime H, Tabeling P and Jousse F 2006 Producing droplets in parallel microfluidic systems *Phys. Rev.* E **74** 046306
[129] Link D R, Anna S L, Weitz D A and Stone H A 2004 Geometrically mediated breakup of drops in microfluidic devices *Phys. Rev. Lett.* **92** 054503
[130] Yeh C H, Chen Y C and Lin Y C 2011 Generation of droplets with different concentrations using gradient-microfluidic droplet generator *Microfluid. Nanofluidics* **11** 245–53
[131] Shen Q Y, Zhang C, Tahir M F, Jiang S K, Zhu C Y, Ma Y G and Fu T T 2018 Numbering-up strategies of micro-chemical process: uniformity of distribution of multiphase flow in parallel microchannels *Chem. Eng. Process.* **132** 148–59
[132] Herdem M S, Mundhwa M, Farhad S and Hamdullahpur F 2018 Multiphysics modeling and heat distribution study in a catalytic microchannel methanol steam reformer *Energy Fuels* **32** 7220–34
[133] Senn S M and Poulikakos D 2004 Tree network channels as fluid distributors constructing double-staircase polymer electrolyte fuel cells *J. Appl. Phys.* **96** 842–52
[134] Hashimoto M, Shevkoplyas S S, Zasońska B, Szymborski T, Garstecki P and Whitesides G M 2008 Formation of bubbles and droplets in parallel, coupled flow-focusing geometries *Small* **4** 1795–805
[135] Li W, Young E W K, Seo M, Nie Z H, Garstecki P, Simmons C A and Kumacheva E 2008 Simultaneous generation of droplets with different dimensions in parallel integrated microfluidic droplet generators *Soft Matter* **4** 258–62
[136] Li W, Greener J, Voicu D and Kumacheva E 2009 Multiple modular microfluidic (M^3) reactors for the synthesis of polymer particles *Lab Chip* **9** 2715–21
[137] Yadavali S, Jeong H H, Lee D and Issadore D 2018 Silicon and glass very large scale microfluidic droplet integration for terascale generation of polymer microparticles *Nat. Commun.* **9** 1222
[138] Kawakatsu T, Kikuchi Y and Nakajima M 1997 Regular-sized cell creation in microchannel emulsification by visual microprocessing method *J. Am. Oil Chem. Soc.* **74** 317–21
[139] Wu J Y, Yadavali S, Lee D and Issadore D A 2021 Scaling up the throughput of microfluidic droplet-based materials synthesis: a review of recent progress and outlook *Appl. Phys. Rev.* **8** 031304
[140] Vladisavljević G T, Ekanem E E, Zhang Z L, Khalid N, Kobayashi I and Nakajima M 2018 Long-term stability of droplet production by microchannel (step) emulsification in microfluidic silicon chips with large number of terraced microchannels *Chem. Eng. J.* **333** 380–91
[141] Vladisavljević G T, Kobayashi I and Nakajima M 2008 Generation of highly uniform droplets using asymmetric microchannels fabricated on a single crystal silicon plate: effect of emulsifier and oil types *Powder Technol.* **183** 37–45
[142] Stolovicki E, Ziblat R and Weitz D A 2018 Throughput enhancement of parallel step emulsifier devices by shear-free and efficient nozzle clearance *Lab Chip* **18** 132–8
[143] Amstad E, Chemama M, Eggersdorfer M, Arriaga L R, Brenner M P and Weitz D A 2016 Robust scalable high throughput production of monodisperse drops *Lab Chip* **16** 4163–72
[144] Sugiura S, Nakajima M, Tong J H, Nabetani H and Seki M 2000 Preparation of monodispersed solid lipid microspheres using a microchannel emulsification technique *J. Colloid Interface Sci.* **227** 95–103
[145] Wang M, Kong C, Liang Q S, Zhao J X, Wen M L, Xu Z B and Ruan X D 2018 Numerical simulations of wall contact angle effects on droplet size during step emulsification *RSC Adv.* **8** 33042–7
[146] Kobayashi I, Takano T, Maeda R, Wada Y, Uemura K and Nakajima M 2008 Straight-through microchannel devices for generating monodisperse emulsion droplets several microns in size *Microfluid. Nanofluidics* **4** 167–77
[147] Hoang D A, Haringa C, Portela L M, Kreutzer M T, Kleijn C R and van Steijn V 2014 Design and characterization of bubble-splitting distributor for scaled-out multiphase microreactors *Chem. Eng. J.* **236** 545–54

[148] Yang C G, Pan R Y and Xu Z R 2015 A single-cell encapsulation method based on a microfluidic multi-step droplet splitting system *Chin. Chem. Lett.* **26** 1450–4
[149] Wu S C, Wu L Y, Chen J, Zhang C B, Liu X D, Chen Y P and Gao W 2023 Splitting behaviors of droplets in fractal tree-shaped microchannels *Int. J. Multiph. Flow* **163** 104440
[150] Chen Y P, Liu X D and Shi M H 2013 Hydrodynamics of double emulsion droplet in shear flow *Appl. Phys. Lett.* **102** 051609
[151] Wang J X, Lai H, Zhong M L, Liu X D, Chen Y P and Yao S H 2023 Design and scalable fabrication of liquid metal and nano-sheet graphene hybrid phase change materials for thermal management *Small Methods* **7** 2300139
[152] Zhou C F, Yue P T and Feng J J 2006 Formation of simple and compound drops in microfluidic devices *Phys. Fluids* **18** 092105
[153] Yu C, Wu L Y, Li L and Liu M F 2019 Experimental study of double emulsion formation behaviors in a one-step axisymmetric flow-focusing device *Exp. Therm. Fluid Sci.* **103** 18–28
[154] Nisisako T, Ando T and Hatsuzawa T 2012 High-volume production of single and compound emulsions in a microfluidic parallelization arrangement coupled with coaxial annular world-to-chip interfaces *Lab Chip* **12** 3426–35
[155] Romanowsky M B, Abate A R, Rotem A, Holtze C and Weitz D A 2012 High throughput production of single core double emulsions in a parallelized microfluidic device *Lab Chip* **12** 802–7
[156] Eggersdorfer M L, Zheng W, Nawar S, Mercandetti C, Ofner A, Leibacher I, Koehler S and Weitz D A 2017 Tandem emulsification for high-throughput production of double emulsions *Lab Chip* **17** 936–42
[157] Zhu P A and Wang L Q 2017 Passive and active droplet generation with microfluidics: a review *Lab Chip* **17** 34–75
[158] Shi Z, Lai X C, Sun C T, Zhang X G, Zhang L, Pu Z H, Wang R D, Yu H X and Li D C 2020 Step emulsification in microfluidic droplet generation: mechanisms and structures *Chem. Commun.* **56** 9056–66
[159] Rodríguez-Rivero C, Del Valle E M M and Galán M A 2011 Development of a new technique to generate microcapsules from the breakup of non-Newtonian highly viscous fluid jets *AIChE J.* **57** 3436–47
[160] Marcali M, Chen X M, Aucoin M G and Ren C L 2022 Droplet formation of biological non-Newtonian fluid in T-junction generators. I. Experimental investigation *Phys. Rev.* E **105** 025105
[161] Zhang Q D, Zhu C Y, Du W, Liu C, Fu T T, Ma Y G and Li H Z 2018 Formation dynamics of elastic droplets in a microfluidic T-junction *Chem. Eng. Res. Des.* **139** 188–96
[162] Mousavi S, Siavashi M and Bagheri M 2023 Comparison of the jet breakup and droplet formation between non-Newtonian and Newtonian fluids *J. Non-Newton. Fluid Mech.* **321** 105093
[163] Luo Q M and Pentzer E 2020 Encapsulation of ionic liquids for tailored applications *ACS Appl. Mater. Interfaces* **12** 5169–76
[164] Santiago R, Lemus J, Moya C, Moreno D, Alonso-Morales N and Palomar J 2018 Encapsulated ionic liquids to enable the practical application of amino acid-based ionic liquids in CO_2 capture *ACS Sustain. Chem. Eng.* **6** 14178–87
[165] Song T Q M, Avelar Bonilla G M, Morales-Collazo O, Lubben M J and Brennecke J F 2019 Recyclability of encapsulated ionic liquids for post-combustion CO_2 capture *Ind. Eng. Chem. Res.* **58** 4997–5007
[166] Hiraga Y, Koyama K, Sato Y and Smith R L 2018 Measurement and modeling of CO_2 solubility in [bmim]Cl—[bmim][Tf_2N] mixed-ionic liquids for design of versatile reaction solvents *J. Supercrit. Fluids* **132** 42–50
[167] Lemus J, Da Silva F F A, Palomar J, Carvalho P J and Coutinho J A P 2018 Solubility of carbon dioxide in encapsulated ionic liquids *Sep. Purif. Technol.* **196** 41–46
[168] Kaviani S, Kolahchyan S, Hickenbottom K L, Lopez A M and Nejati S 2018 Enhanced solubility of carbon dioxide for encapsulated ionic liquids in polymeric materials *Chem. Eng. J.* **354** 753–7
[169] Wang P P, Zhu J M, Tang J C, Kang J and Shi L 2022 Morphology and CO_2 adsorption performance of novel ionic liquid microcapsules containing [Bmim][PF_6] *Chem. Eng. Res. Des.* **187** 633–44
[170] Moore T, Rim G, Park A H A, Mumford K A, Stevens G W and Webley P A 2022 Encapsulation of highly viscous CO_2 capture solvents for enhanced capture kinetics: modeling investigation of mass transfer mechanisms *Chem. Eng. J.* **428** 131603
[171] Mohamed A, Krokidas P and Economou I G 2018 CO_2 selective metal organic framework ZIF-8 modified through ionic liquid encapsulation: a computational study *J. Comput. Sci.* **27** 183–91
[172] Avelar Bonilla G M, Morales-Collazo O and Brennecke J F 2019 Effect of water on CO_2 capture by aprotic heterocyclic anion (AHA) ionic liquids *ACS Sustain. Chem. Eng.* **7** 16858–69
[173] Wang H M, Zhu J M, Tan L, Zhou M and Zhang S Q 2020 Encapsulated ionic liquids for CO_2 capture *Mater. Chem. Phys.* **251** 122982
[174] Moya C, Alonso-Morales N, Gilarranz M A, Rodriguez J J and Palomar J 2016 Encapsulated ionic liquids for CO_2 capture: using 1-butyl-methylimidazolium acetate for quick and reversible CO_2 chemical absorption *ChemPhysChem* **17** 3891–9
[175] Xue C F, Zhu H Y, Du X, An X W, Wang E Y, Duan D H, Shi L J, Hao X G, Xiao B and Peng C J 2017 Unique allosteric effect-driven rapid adsorption of carbon dioxide in a newly designed ionogel [P_{4444}][2-Op]@MCM-41 with excellent cyclic stability and loading-dependent capacity *J. Mater. Chem.* A **5** 6504–14
[176] Knipe J M, Chavez K P, Hornbostel K M, Worthington M A, Nguyen D T, Ye C W, Bourcier W L, Baker S E, Brennecke J F and Stolaroff J K 2019 Evaluating the performance of micro-encapsulated CO_2 sorbents during CO_2 absorption and regeneration cycling *Environ. Sci. Technol.* **53** 2926–36
[177] Li L R, Jung H S, Lee J W and Kang Y T 2022 Review on applications of metal–organic frameworks for CO_2 capture and the performance enhancement mechanisms *Renew. Sustain. Energy Rev.* **162** 112441
[178] Zhang F, Wei Y Y, Wu X T, Jiang H Y, Wang W and Li H X 2014 Hollow zeolitic imidazolate framework nanospheres as highly efficient cooperative catalysts for [3+3] cycloaddition reactions *J. Am. Chem. Soc.* **136** 13963–6
[179] Carné-Sánchez A, Imaz I, Cano-Sarabia M and Maspoch D 2013 A spray-drying strategy for synthesis of nanoscale metal–organic frameworks and their assembly into hollow superstructures *Nat. Chem.* **5** 203–11
[180] Zhang L J, Liand F and Luo L F 2018 Preparation methods of metal organic frameworks and their capture of CO_2. *IOP Conf. Ser.: Earth Environ. Sci.* **108** 042104
[181] Hsieh P F, Law Z X, Lin C H and Tsai D H 2022 Understanding solvothermal growth of metal-organic framework colloids for CO_2 capture applications *Langmuir* **38** 4415–24
[182] Ameloot R, Vermoortele F, Vanhove W, Roeffaers M B J, Sels B F and De Vos D E 2011 Interfacial synthesis of

hollow metal-organic framework capsules demonstrating selective permeability *Nat. Chem.* **3** 382–7
[183] Wu S T, Xin Z, Zhao S C and Sun S T 2019 High-throughput droplet microfluidic synthesis of hierarchical metal-organic framework nanosheet microcapsules *Nano Res.* **12** 2736–42
[184] Couck S, Denayer J F M, Baron G V, Rémy T, Gascon J and Kapteijn F 2009 An amine-functionalized MIL-53 metal−organic framework with large separation power for CO_2 and CH_4 *J. Am. Chem. Soc.* **131** 6326–7
[185] Bae Y S, Spokoyny A M, Farha O K, Snurr R Q, Hupp J T and Mirkin C A 2010 Separation of gas mixtures using Co(II) carborane-based porous coordination polymers *Chem. Commun.* **46** 3478–80
[186] Cavenati S, Grande C A, Rodrigues A E, Kiener C and Müller U 2008 Metal organic framework adsorbent for biogas upgrading *Ind. Eng. Chem. Res.* **47** 6333–5
[187] Caskey S R, Wong-Foy A G and Matzger A J 2008 Dramatic tuning of carbon dioxide uptake via metal substitution in a coordination polymer with cylindrical pores *J. Am. Chem. Soc.* **130** 10870–1
[188] Aines R D, Spaddaccini C M, Duoss E B, Stolaroff J K, Vericella J, Lewis J A and Farthing G 2013 Encapsulated solvents for carbon dioxide capture *Energy Proc.* **37** 219–24
[189] Yew M 2021 *Synthesis of Functional Materials for Carbon Capture via Microfluidic Platform* (University of Nottingham)
[190] Nabavi S A, Vladisavljević G T, Gu S and Manović V 2016 Semipermeable elastic microcapsules for gas capture and sensing *Langmuir* **32** 9826–35
[191] Wang D Y, Yu W, Gao M, Liu K, Wang T, Park A and Lin Q 2018 A 3D microfluidic device for carbon capture microcapsules production *2018 IEEE Micro Electro Mechanical Systems* (*Belfast, UK*) (IEEE) pp 1193–6
[192] Shi J S, Cui H M, Xu J G and Yan N F 2022 Carbon spheres synthesized from $KHCO_3$ activation of glucose derived hydrochar with excellent CO_2 capture capabilities at both low and high pressures *Sep. Purif. Technol.* **294** 121193
[193] Rama S, Zhang Y, Tchuenbou-Magaia F, Ding Y L and Li Y L 2019 Encapsulation of 2-amino-2-methyl-1-propanol with tetraethyl orthosilicate for CO_2 capture *Front. Chem. Sci. Eng.* **13** 672–83
[194] Finn J R and Galvin J E 2018 Modeling and simulation of CO_2 capture using semipermeable elastic microcapsules *Int. J. Greenhouse Gas Control* **74** 191–205
[195] Yew M, Ren Y, Koh K S, Sun C G, Snape C and Yan Y Y 2019 Synthesis of microcapsules for carbon capture via needle-based droplet microfluidics *Energy Proc.* **160** 443–50